BOREAS An international journal of Quaternary research

Palaeoclimatic and regional implications of Older Dryas and Younger Dryas local glacier activity in the low-Arctic valley Finnkongdalen, Andøya, northern Norway

HENRIK LØSETH JANSEN, SVEIN OLAF DAHL, HENRIETTE LINGE, JOSTEIN BAKKE, PÅL RINGKJØB NIELSEN AND BJØRN CHRISTIAN KVISVIK

BOREAS

Jansen, H. L., Dahl, S. O., Linge, H., Bakke, J., Nielsen, P. R. & Kvisvik, B. C. 2023 (April): Palaeoclimatic and regional implications of Older Dryas and Younger Dryas local glacier activity in the low-Arctic valley Finnkongdalen, Andøya, northern Norway. *Boreas*, Vol. 52, pp. 168–193. https://doi.org/10.1111/bor.12609. ISSN 0300-9483.

Continuous glacier margin and equilibrium-line altitude fluctuations of a former glacier on central Andøya, northern Norway, are reconstructed during the Lateglacial based on moraines and AMS ^{14}C-dated sediments from the distal glacier-fed lake Ner-Finnkongdalsvatnet. The results indicate that a valley glacier occupied the entire valley during the Last Glacial Maximum (before 21 970±620 cal. a BP). The glacier remained large throughout the early Lateglacial until a significant glacier retreat took place about 14 300±330 cal. a BP. Major advances occurred during the Older Dryas (OD) and during the Younger Dryas (YD), while minor advances are suggested to have taken place during the Intra Allerød Cold Period and the Late Allerød Cooling. Additionally, three smaller glacier retreats/re-advances within the YD are suggested to have taken place, the latter being the largest. The glacier re-formations/advances during the Lateglacial are consistent with increases in temperature, and they are thus suggested to be the result of increased winter precipitation. Comparing the results with relevant glacier and sea-surface temperature records, a south–north migration of storm tracks may have occurred between 12 100–11 810±220 cal. a BP. The high temporal resolution of local glacier activity in Finnkongdalen improves our understanding of the climate forcing of the regional glacier fluctuations of the northwestern sector of the Scandinavian Ice Sheet during the Skarpnes- (OD) and Tromsø-Lyngen (YD) re-advances.

Henrik Løseth Jansen (henrik.jansen@uib.no), Pål Ringkjøb Nielsen and Bjørn Christian Kvisvik, Department of Geography, University of Bergen, Fosswinckelsgate 6, N-5007 Bergen, Norway; Svein Olaf Dahl, Department of Geography, University of Bergen, Fosswinckelsgate 6, N-5007 Bergen, Norway and Bjerknes Centre for Climate Research, N-5020 Bergen, Norway; Henriette Linge, Department of Earth Science, University of Bergen, N-5020 Bergen, Norway and Bjerknes Centre for Climate Research, N-5020 Bergen, Norway; Jostein Bakke, Department of Earth Science and Bjerknes Centre for Climate Research, University of Bergen, N-5020 Bergen, Norway and Bjerknes Centre for Climate Research, N-5020 Bergen, Norway; *received 28th February 2022, accepted 16th October 2022.*

The net mass balance of small glaciers is very sensitive to changes in the interaction between ablation season temperature and regional distribution of snow during the accumulation season (e.g. Dahl & Nesje 1992). Hence, knowledge of the presence and extent of small Arctic and alpine glaciers gives an insight into the present and past regional distribution of prevailing temperature, precipitation and wind patterns, and thereby increases our understanding of global atmospheric and oceanic circulation systems.

The low-Arctic North Atlantic coastal region of northern Norway is of particular interest for studying past climate changes because the present day winter air temperature is high considering the high latitude (Weibull *et al*. 2022), and the proximity to the Norwegian Atlantic Current (NwAC) (Fig. 1). Together with the North Atlantic storm track pattern, this acts as a major provider of heat and moisture to the Arctic, and the observed Arctic amplification of the ongoing increase in global temperature (Serreze & Barry 2011; Leclercq & Oerlemans 2012) is suggested to be reflected in the rapid retreat of Scandinavian glaciers from the 19th century onwards (Nesje *et al*. 2008).

The general deglaciation course of the NW sector of the Scandinavian Ice Sheet (SIS) during the Lateglacial is well mapped on the continental shelf (Vorren & Elvsborg 1979; Vorren & Plassen 2002; Dahlgren & Vorren 2003; Rørvik *et al*. 2010; Rydningen *et al*. 2013; Vorren *et al*. 2013, 2015; Laberg *et al*. 2018) and along the coast of northern Norway (e.g. Andersen 1968, 1975; Vorren *et al*. 1988; Møller *et al*. 1992; Bakke *et al*. 2005). Due to the proximity to the shelf edge and the rapid retreat of a glacier front in a marine environment, the northern tip of Andøya is well known for its old sediments undisturbed by glacial overriding, possibly going back to 26.7 cal. ka BP (Fig. 1; Vorren 1978; Vorren *et al*. 2013; Alsos *et al*. 2020). The area is also known for the presence of *Pinus*, *Picea* and *Betula* during and just after the LGM (Kullman 2006; Parducci *et al*. 2012; Alsos *et al*. 2020).

Finnkongdalen is a SE-NW orientated valley located in west-central Andøya (latitude 69°N, longitude 15°E), the northernmost island of the Vesterålen archipelago in low-Arctic Norway (Fig. 1). The catchment (3.2 km^2) contains two lakes, Øver- (upper) and Ner- (lower) Finnkongdalsvatn (Fig. 2). The lakes are overdeepenings separated by a till-covered bedrock sill. The majority of the local bedrock in the drainage area consists of gabbro and gabbronorite (~80%), while granitic dykes (~20%) occur in the former bedrock types in the southern and the western parts of the drainage area (Henningsen & Tveten 1998).

DOI 10.1111/bor.12609

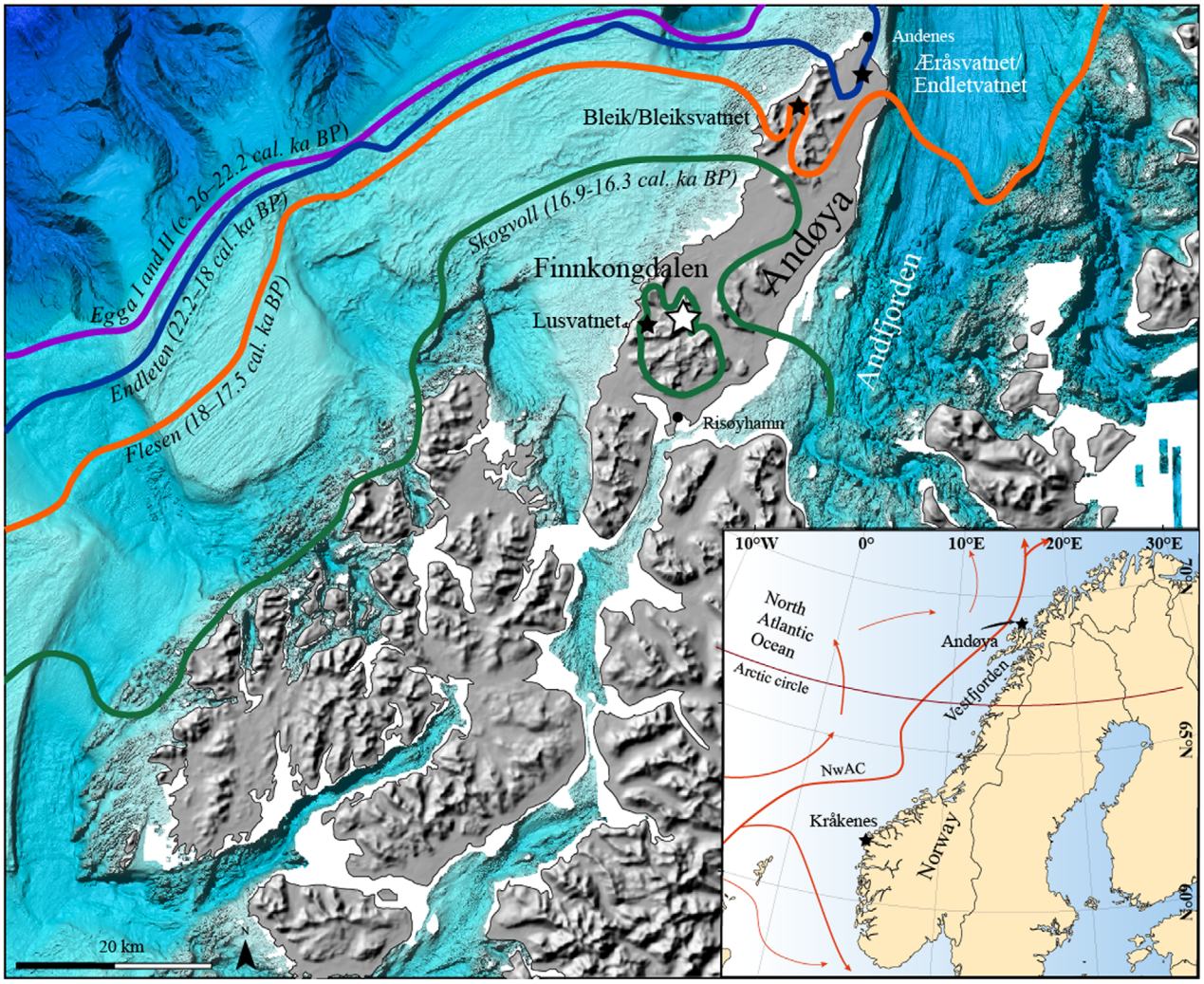

Fig. 1. Andøya is located in Vesterålen on the west coast of northern Norway. Northern Andøya is known for its proximity to the shelf-edge and thus the ice-margin during past major advances of the SIS. Coloured lines show reconstructed maximum front positions (Vorren *et al.* 2015). Note the green 'Skogvoll' line enclosing the mountain massif in which Finnkongdalen is located, indicating a nunatak between 16.9–16.3 cal. ka BP. Other sites discussed and the Norwegian Atlantic Current (NwAC) are shown on the inset maps of Andøya and the Scandinavian peninsula. Bathymetric surface DEM downloaded from Norwegian Geological Survey. Terrestrial surface DEM downloaded from Norwegian Mapping Authority.

The main objective of this paper is to reconstruct the timing and continuous ELA variations of a small local glacier in Finnkongdalen at the low-Arctic western coast of central Andøya, northern Norway (Fig. 1). The ELA reconstruction is then used to quantify regionally representative variations in solid winter precipitation during the Lateglacial, which are compared with other relevant glacier-, temperature-, sea-surface temperature (SST)- and sea-ice cover records in the North Atlantic region.

Material and methods

Quaternary geological mapping, GPR and coring

Landforms and surface deposits in the Finnkongdalen drainage area were mapped in the field and categorized according to primary depositional processes. The mapping was conducted with emphasis on landscape processes, which have the potential to significantly influence the depositional environment in Ner-Finnkongdalsvatnet, such as glacial- and slope-related processes. Results from the field study were cross-checked and refined using terrain hillshading based on high resolution elevation data (Lidar: 2 pt m^{-2}) made available by the Norwegian Mapping Authority (Kartverket 2022). The map was produced in ArcGIS and refined using Adobe Illustrator.

GPR-profiling of lake bottom sediments was done using a Ramac GPR with 50 and 100 MHz RTA antennae from Malå GeoScience (Larsen 2010). Profiling was conducted from rubber boats. Antennas were either strapped to, or trailed behind the boat, inside a waterproof plastic tube. The GPR profiles were

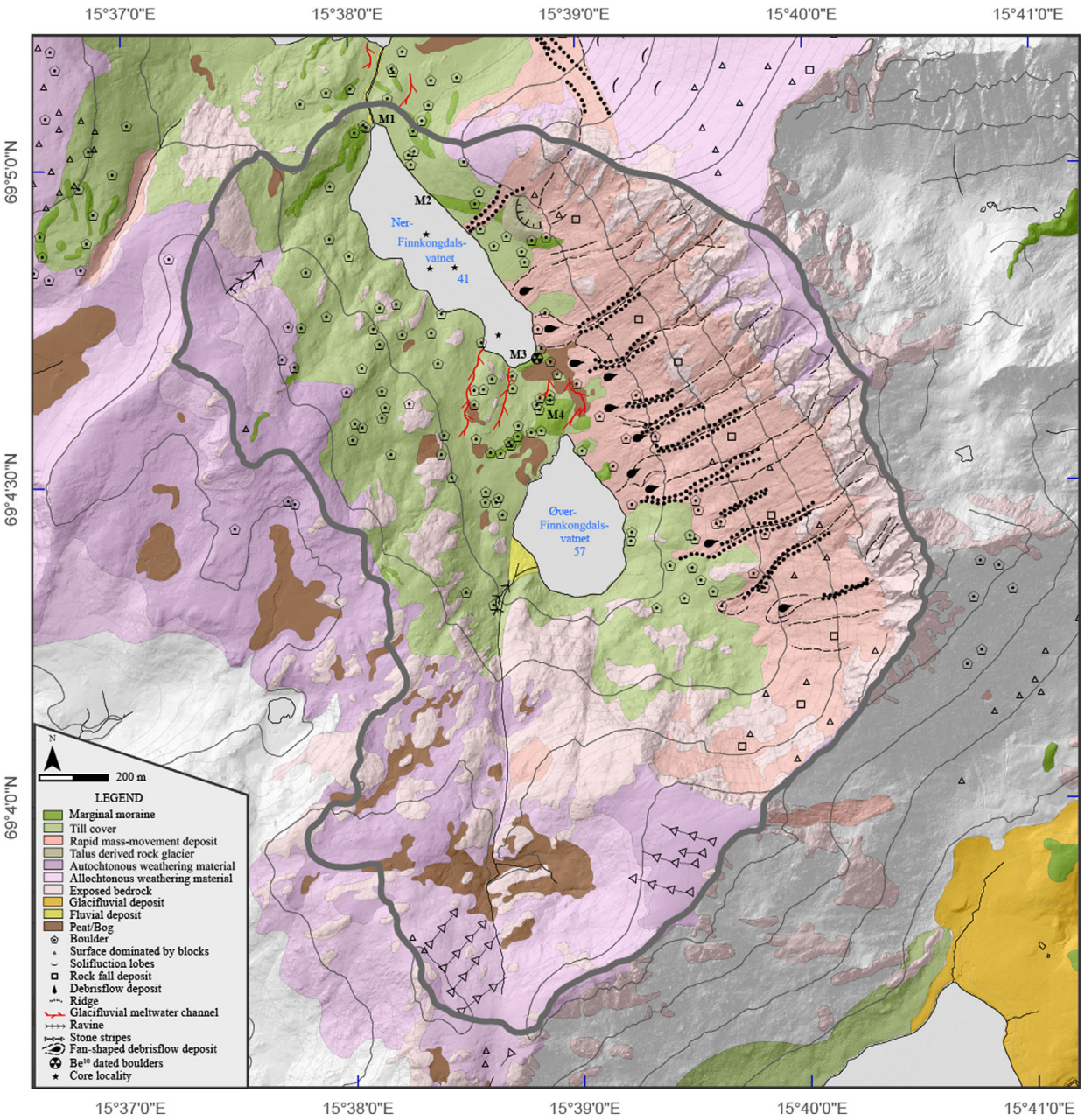

Fig. 2. Quaternary geological map showing the Ner-Finnkongdalsvatnet catchment. The catchment was mapped with emphasis on processes that influence the depositional environment in the lake. Thick, grey line outlines the catchment area of Ner-Finnkongdalsvatnet. Colours and symbols follow the standard given by the Geological Survey of Norway. Elevation data (NDH Andøy 2 pt) from Norwegian mapping authority.

processed in RadExplorer. Water depth and relative sediment thickness were calculated by interpolation, using the Topo-to-raster tool in ArcGIS.

In total, nine cores (NFP 109–NFP 909) were collected from Ner-Finnkongdalsvatnet from lake ice using a piston-corer (Nesje 1992a). The location for each coring site was chosen based on the bathymetry of the lake and relative sediment thickness, as well as the relative distance to important sources of sediment input from former glacial meltwater streams (Dahl *et al.* 2003). Two cores were examined in detail in this study. Core NFP 409 was collected from a 2–4 m deep area near the main source of sediments to the lake and NFP 809 was collected further away from the main inlet to the lake (Fig. 4).

^{10}Be dating

The samples collected for ^{10}Be dating are glacially transported boulders situated on a marginal moraine (Fig. 2). Samples were collected using hammer and chisel. Sample locations and elevations were recorded in the field with a hand-held GPS. Clinometer measurements were

taken for each sample for determination of the site-specific topographic shielding. Field notes on the sample thickness, as well as the likelihood for erosion or snow shielding were noted. The samples were analysed according to procedures described by Kohl & Nishiizumi (1992), Child *et al.* (2000), Xu *et al.* (2010), Borchers *et al.* (2016), Lifton *et al.* (2014) and Marrero *et al.* (2016) (Data S1).

Surface exposure ages were calculated from the ^{10}Be concentrations using the CRONUScalc program (Marrero *et al.* 2016). We report ^{10}Be surface exposure ages ($\pm 1\sigma$) calculated according to the Sa scaling framework (Lifton *et al.* 2014; Borchers *et al.* 2016), the ^{10}Be production rate derived from the primary calibration data set of Borchers *et al.* (2016), and assuming 1 mm ka^{-1} erosion. The analytical (internal) uncertainty is used when comparing results internally (i.e. ^{10}Be data only), whereas the total uncertainty (combined analytical and production rate uncertainties) is used when comparing the results with ages obtained using other cosmogenic nuclides or other dating methods.

Lake sediment cores

Laboratory analyses. – All cores were analysed for magnetic susceptibility (MS) with a Bartington MS2E point sensor at 2-mm intervals to correlate the cores (Thompson *et al.* 1975).

In addition to MS, NFP 409 and NFP 809 were analysed for loss on ignition (LOI), dry bulk density (DBD) and X-ray fluorescence (XRF). Grain-size analysis was done on NFP 809.

LOI is a measure of the organic content in the bulk sediment, and has been widely used as an inverse proxy for glacial erosion in lake catchments (Karlén 1976, 1981; Nesje *et al.* 2001).

DBD depends on the density of the minerogenic grains and porosity and is a measure of the relative amount of non-organic material in the bulk sediment. Variations in DBD have been used as a proxy for variations in glacier magnitude in proglacial lakes (e.g. Bakke *et al.* 2005, 2010).

LOI and DBD were analysed by extracting volume specific samples (1 cm^3) at 0.5-cm intervals, which were dried at 105 °C for 12 h and weighed to obtain the DBD. The samples were then combusted at 550 °C for an hour and left to cool in a desiccator. Afterwards they were weighed, and the LOI was calculated according to Heiri *et al.* (2001).

Variations in geochemical composition, obtained from an XRF-analysis, can be used to infer sedimentological, diagenetic and environmental changes (Croudace *et al.* 2006). Variations in single elements alone or relative to other elements may be linked to temporal changes of a single or a set of processes in the depositional environment (Haug *et al.* 2001; Bakke *et al.* 2009).

Biogenic processes may affect the variability of both Si and Ca, while the K-count rate may be influenced by varying amounts of detrital clay (Croudace *et al.* 2006). As Ti is redox insensitive and not affected by biogenic processes or variations in grain size and water content (porosity), it is commonly recognized as a good indicator of terrestrial erosion (Haug *et al.* 2001; Bakke *et al.* 2009).

The XRF analysis was conducted with an interval of 200 µm on an ITRAX core scanner (cf. Croudace *et al.* 2006), equipped with a Cr-tube at the department of Earth Sciences, University of Bergen.

Grain-size analysis was performed on the grain sizes from clay to fine sand using Micromeritics Sedigraph 5100 and the sample statistics were calculated using Gradistat v. 8 (Webb & Orr 1997; Blott & Pye 2001).

AMS radiocarbon ages. – The age-depth model is based on dated levels in NFP 109, NFP 209 and NFP 809. Terrestrial plant macrofossils for AMS ^{14}C-dating were carefully handpicked and cleaned from 1-cm-thick slices of the bulk sediments. The samples were dried at 50 °C for 24 h before submission for AMS ^{14}C-dating at the Poznań Radiocarbon Laboratory. Macrofossils were generally small and scarce (<0.4 mg TOC) and the dates Poz-48489 and Poz-48494 are based on the combined mass of macrofossils from 4- and 3-cm sediment slices, respectively, as they were too small to be dated individually. For the majority of samples it was not possible to identify individual species. Still, all samples were identified as terrestrial plant fragments.

The radiocarbon ages were calibrated using the IntCal20 calibration curve (Reimer *et al.* 2020). The age–depth relationship was modelled in R (R Core Team 2021), using Clam v 2.4.0 (Blaauw 2010). Best-fit estimates were defined as a weighted average of 1000 iterations, after excluding models with age-depth reversals.

Principal component analysis. – Principal component analysis (PCA) is an ordination technique that is commonly applied on multivariate data sets to identify patterns of variability in the data set (Birks 1987; Vasskog *et al.* 2012; Bakke *et al.* 2013). A PCA was conducted on Si, K, Ca count rates, MS, LOI and DBD from NFP 409 and NFP 809. Compositional data, such as grain-size percentages and the Fe/Ti ratio were not included to avoid the closure problem (Birks 1987). The analysis was conducted in AnalySeries 2.0.4.2 (Pailard *et al.* 1996).

The sediment parameters from the cores, which were collected at localities relative to different sediment sources, are therefore interpreted with respect to the results from Quaternary geological mapping.

Reconstructions of glacier size, ELA and precipitation

The reconstructed glacier outlines are based on the mapped moraines, as well as theoretical surface profiles along the central flowline, using Benn & Hulton (2010)'s steady-state model. This model calculates the ice-surface elevation along the central flowline, based on the relationship between the shear stress and rate of ice deformation.

ELA calculations were conducted by using the ELA calculation tool written by Pellitero *et al.* (2015) in ArcGIS. This tool allows for ELA calculations based on a reconstructed glacier surface raster, which is interpolated from the modelled surface profiles and constrained in extent based on marginal moraines and a digital elevation model (DEM) of the valley.

Accumulation-area ratio (AAR) is a useful calculation method for easily calculating the ELA of a glacier, using typical values for the relative distribution of the accumulation and the ablation area. The reconstructed glaciers of Finnkongdalen was calculated with a presumed AAR of 0.6±0.05, which is common on small, steady-state cirque and valley glacier systems (Porter 1975). The accumulation × area balance-ratio (AABR) method also includes glacier hypsometry and may potentially yield more precise calculations if accurate estimates of the former balance ratio (BR) are applied. Oien *et al.* (2021) found a very strong correlation between the calculated AABR ELA and measured zero-net balance ELAs of modern Scandinavian glaciers, using a mean regional BR of 1.5 ($r^2 = 0.92$, $n = 18$) (Oien *et al.* 2021). A BR of 1.5 is therefore applied to the AABR-ELA calculations (Osmaston 2005; Rea 2009; Oien *et al.* 2021). The BR of glaciers depends on climatic factors such as temperature regime. The relative importance of wind-blown snow is reduced with the increasing magnitude of small cirque/valley glaciers, as shown by Nielsen *et al.* (2016a) for a cirque glacier in Lofoten.

ELA estimates for G1, G3 and G4 were adjusted for the contemporaneous relative sea level at the suggested time of moraine formation (Rasmussen 1984; Vorren *et al.* 1988; Møller 1989).

A linear relationship was established between moraine-based ELA reconstruction and the variability of Ti in the lithology of lake Ner-Finnkongdalsvatnet. A continuous record of former ELA was produced by applying the relationship to the continuous record of Ti in the lithology.

The contribution of snow at the ELA was quantified by combining the reconstructed continuous ELA record with an independent proxy for local mean ablation season temperatures (Birks *et al.* 2014), using the Liestøl relationship (Liestøl 1967). The Liestøl equation ($A = 0.915\ e0.339t$) expresses the close exponential relationship ($R^2 = 0.989$, $p < 0.0001$) between mean ablation season temperature (t) (1 May–30 September) and annual winter precipitation as snow in metres water equivalents (m w.e.) (A) at the ELA of Norwegian glaciers existing in continental to maritime climate regimes (Liestøl 1967; Lie & Paasche 2006). It implies that if an independent proxy for mean ablation season temperature at a former ELA is known, mean annual winter precipitation as snow can be quantified (Dahl & Nesje 1992, 1996). If only reconstructed July temperature (T_{Jul}) estimates are available, they must be recalculated to mean ablation season temperature before being corrected for the environmental atmospheric lapse rate and land uplift relative to the contemporaneous relative sea level (Dahl & Nesje 1996; Paasche *et al.* 2007).

The Liestøl relationship and altitude corrected ablation season temperature yield the accumulation of snow at the ELA. However, this includes the leeward accumulation of snow and snow avalanches as well as regional accumulation season precipitation. The regionally representative winter precipitation at sea level is found by correcting the contribution of snow at the ELA for the effect of leeward accumulation of wind-transported snow, using a D/A ratio of 3.83. The D/A ratio is an easy way of estimating the potential for leeward accumulation of snow by wind, including snow-avalanches, on cirque or small valley glaciers (Dahl *et al.* 1997; Nielsen *et al.* 2016a). The ratio is based on the total drainage area (D) above the ELA (the potential surface where snow can be deposited) and the reconstructed accumulation area of the glacier (A). A D/A ratio of 3.83 is applied when calculating the effect of wind-transported snow on the winter balance at the ELA (Fig. 10D) and a relative land uplift of up to 35 m (Vorren *et al.* 2013).

The quality of the winter precipitation reconstruction (output) relies on the degree of precision and accuracy of the estimated ablation season temperature on the ELA. Uncertainties regarding the method itself and necessary corrections of proxy records to fit the requirements of using the Liestøl relationship to infer winter precipitation, may introduce potential sources of error that are difficult to quantify. The output must therefore be interpreted with caution.

Results

Quaternary geological mapping, glacier reconstructions and ELA

Several mounds and ridges consisting of a boulder rich diamicton were observed at the valley floor (Fig. 4). The ridges vary in height between 0.5–4 m and are organized as single ridges or a complex of mounds and ridges within a discrete area. Due to the unsorted character of the sediment and shape of the ridges, they are interpreted as a sequence of four marginal moraines (M1–4; Figs 2, 4).

M1, the farthest downvalley of the four mapped moraines, consists of separate ridges on each valley side that are interpreted as one ice-marginal position. The eastern part of M1 is composed of several mounds and ridges, separated by glacifluvial channels. The western part of M1 is a well-defined ridge situated on the crest of a small valley headland and can be followed approximately 130 m upvalley along the western valley side. This 1–1.5 m high ridge is situated on a slope and is not well defined.

M2 is a complex of three separate ridges along the NE valley side and can be followed for roughly 350 m. The ridge system is incised by a prominent debrisflow track

and levees. A rock glacier (described below) has propagated across a section of the ridge (Figs 2, 4).

The moraine M3 consists of a single ridge cut in two by a glacifluvial meltwater channel. M3 is the most prominent of the moraine ridges, rising 4 m from the lake to the crest.

M4 is a complex of several mounds and ridges ranging in height between 1–4 m situated on the sill between the two lakes. The stream that runs between Øver- and Ner-Finnkongdalsvatnet has incised the western part of the moraine, while the eastern part has been modified by debrisflows from the NE valley side. The bedrock sill between M3 and M4 is draped with a hummocky diamicton, interpreted as till.

A lobe-shaped landform with a steep front towards the valley, and consisting of mostly angular boulders, is mapped beneath a talus fan on the NE valley side at an altitude from 65 to 109 m a.s.l. An oval central depression of 2 m is observed on the lower part of the landform, and a less distinct depression of 1 m in the upper part. Due to the characteristic shape, material composition and location, it is interpreted to be a relict talus-derived rock glacier. The rock glacier is located proximal to the interpreted M1 glacier margin position and partly overruns the interpreted M2 moraine complex (Fig. 2).

The elevated area in the southernmost part of the study area and the gently sloping plateau surface in the western parts are both dominated by periglacial features, including a continuous cover of weathering material and scattered gelifluction lobes and stone stripes (Fig. 2).

Several distinct fan-shaped avalanche deposits cover the entire NE and S valley sides (Fig. 2). Clearly distinguishable levees along the avalanche tracks, as well as lobate features, indicate that the fans were formed by coarse debris flows (Blikra & Nemec 1998). The debrisflow fan north of M4 (Figs 2, 4) partly covers the upper part of this moraine, and small overspills of debris flow material are observed on the proximal slope of M3. GPR profiles across the proximal basin portion of Ner-Finnkongdalsvatnet indicate an irregular stratigraphical unit in the underlying sediments of the northern section of this sub-basin (Fig. 4). The stratigraphical unit extends roughly 50 m into the lake from the E-NE lake shore and is characterized by an undulating sediment surface, numerous point reflectors, as well as a generally chaotic structure of reflectors. This is suggested to indicate boulders imbedded in generally poorly sorted sediments. The GPR profile illustrated in Fig. 4 extends from the northern lake shore, where two debrisflow fans extend into the lake. It is therefore suggested that the stratigraphical unit identified in the GPR profiles is the extension of a debrisflow fan that has propagated into the lake.

^{10}Be-dated boulders

The ^{10}Be ages of two boulders on M3 are calculated to 13.3±1.2 ka (FIN0903) and 12.4±1.3 ka (FIN0904), respectively (Table 1, Fig. 9A).

Table 1. Field and laboratory data, and exposure ages from the Finnkongdalen samples.

	Sample	
	FIN 0903	FIN 0904
Elevation (m a.s.l.)	44	45
Sample type	Moraine boulder	Moraine boulder
Lithology	Granitic gneiss	Granitic gneiss
Latitude, longitude (°N, °E)	69.0783, 15.6471	69.0783, 15.6475
Shielding factor[1]	0.9677	0.9677
Thickness[2] (cm) (factor)	1.5 (0.9877)	2.0 (0.9836)
Quartz[3,4] (g)	22.302	21.594
Be carrier[5] (g)	0.2281	0.2220
^{10}Be/^{9}Be[6,7] ($\times10^{-15}$)	96.57±2.94	91.47±5.76
^{10}Be/^{9}Be^{blanks} ($\times10^{-15}$)	4.24±0.61	4.25±0.79
^{10}Be conc.[7,8,9] (10^4 at g^{-1} SiO_2)	6.46±0.26	6.00±0.42
^{10}Be age[7,10,11] ka±total error (analytical error)	13.3±1.2 (0.6)	12.4±1.3 (1.0)

[1]Geometric shielding correction was computed after Dunne *et al.* (1999).
[2]Sample thickness measured from the surface. Correction factor calculated assuming an exponential reduction in ^{10}Be production rate with depth (Gosse & Phillips 2001; Balco *et al.* 2008).
[3]All samples processed and measured at SUERC.
[4]All samples use a density value of 2.7 g cm^{-3}.
[5]Carrier concentration: 980.4 mg g^{-1}.
[6]Isotope ratios normalized to the NIST SRM 4325 ^{10}Be standard with a nominal value of ^{10}Be/^{9}Be = 3.06×10^{-11} (NIST 1990).
[7]Uncertainties are reported at the 1σ confidence level.
[8]Procedural blank values used to correct for background.
[9]Propagated uncertainties include error in the blank and counting statistics.
[10]Ages calculated using the CRONUS Earth web calculator COSMOcalc version 2.0 (Marrero *et al.* 2016). Propagated errors in the calculated ages include uncertainties of the ^{10}Be production rate and of the ^{10}Be decay constant. Errors in parentheses are analytical errors only.
[11]^{10}Be surface exposure ages have been calculated assuming a constant erosion rate of 1 mm ka^{-1} of the boulder surfaces.

No correction for snow cover has been applied here because no continuous modern records of snow-depth are available due to no complete modern-day snow cover records for this area. The results may therefore slightly underestimate the age of exposure. Sample FIN0904 was collected from a boulder surface with some vegetation cover (heather, moss), which could account for the slightly lower ^{10}Be age.

Although higher erosion rates have been found on localities with chemically 'unstable' bedrock surfaces along the coast of Norway (Andersen *et al.* 2022), a relatively modest erosion rate of 1 mm ka^{-1} has been applied (e.g. Johnsen 2020; Anjar *et al.* 2021) as the sample material did not show any signs of extraordinary weathering.

A sea-level correction has not been performed on the present data set because the analysed surfaces are either older than the known sea-level history or only affected by minor (±10 m) fluctuations.

Glacier and ELA reconstruction

Three ice-thickness models (Fig. 3A; G1, G3 and G4) based on the ice-marginal positions M1, M3 and M4,

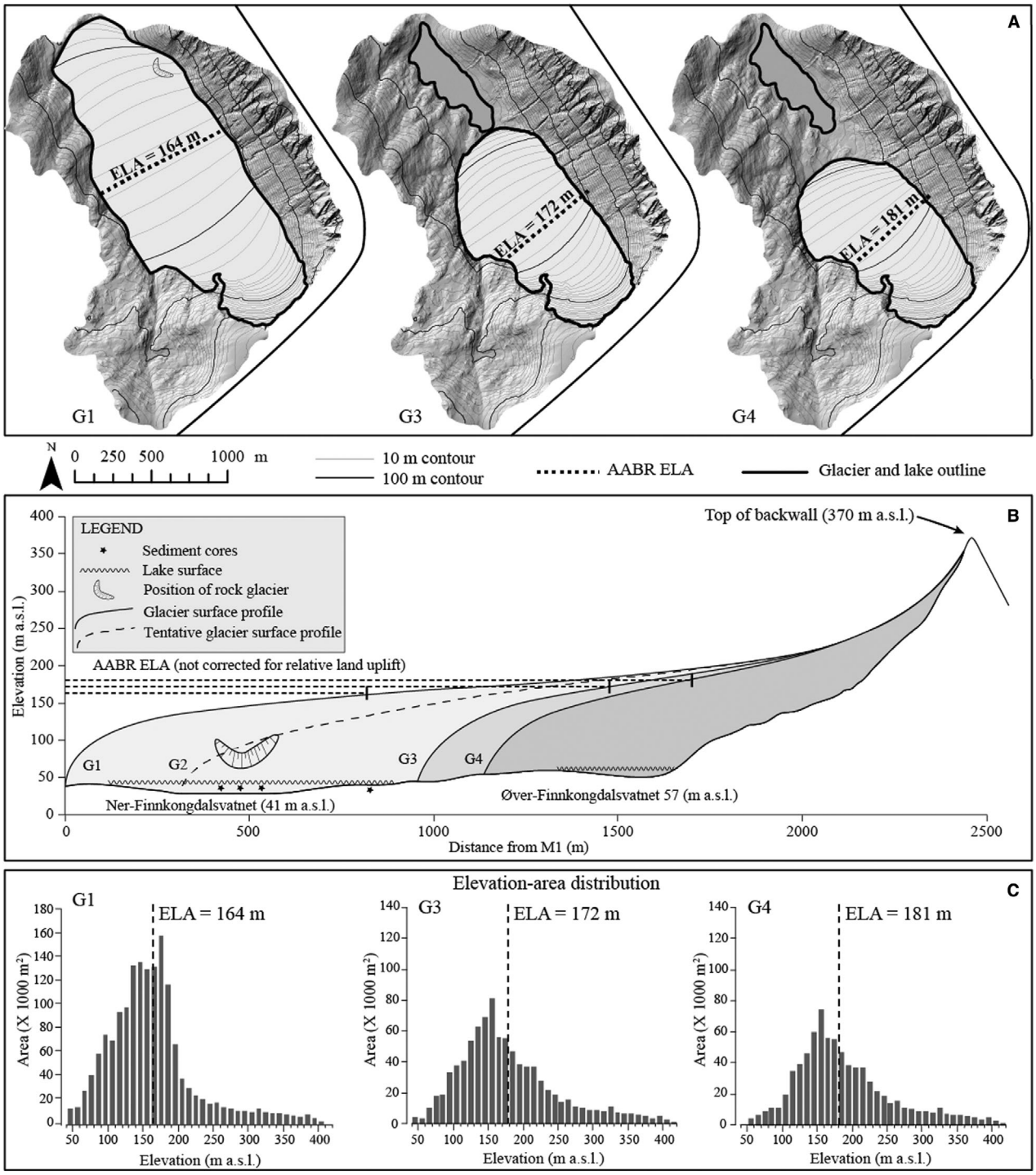

Fig. 3. Modelled glaciers named G1–G4 based on the four moraine sequences M1–M4, respectively. A. Reconstructed area extent. B. Reconstructed ice-surface profiles along the suggested central flowlines of G1–G4. C. Reconstructed hypsometry of G1, G3 and G4. The elevation axis in B and C is based on the present sea level. Note that even slight changes in AABR ELA result in major changes in glacier hypsometry and thus area extent.

respectively, predict that the ice surface had a near vertical front and a more gently sloping surface (7–8°) in the middle part of the glacier. Furthermore, the models indicate steep ice surfaces (<60°) extending to the top of the backwall at 370 m a.s.l. (Fig. 3). Although morphological evidence of ice-marginal positions is absent in the upper reaches, the modelled ice surface matches the course of the moraines near the front.

Table 2. Reconstructed glacier parameters based on M1 (G1), M3 (G3) and M4 (G4).

	M1 (G1)	M3 (G3)	M4 (G4)
^{10}Be age (ka)	–	13.3±1.2 (0.6)/12.4 ±1.3 (1.0)	
Suggested age (cal. a BP±2σ)[1]	≥14 300±330	13 910±140–14 070±180	11 645±110–11 810±220
AABR ELA (m a.s.l.– BR = 1.5)[2]	164±5	172±5	181±5
AAR ELA (m a.s.l.– AAR = 0.6±0.05)	168±13	166±10	175±10
Glacio-isostatic uplift since formation (m)[3]	30	25	9
Corrected AABR ELA (m a.s.l.)	134±5	147±5	172±5
Corrected AAR ELA (m a.s.l.)	138±13	141±10	166±10
Horizontal length (m)	2420	1480	1300
Glacier area (km^2)	1.55	0.89	0.77

[1]The timing of M3 and M4 is based on the dated stratigraphy in Ner-Finnkongdalsvatnet.
[2]From Oien *et al.* (2021).
[3]From Møller (1989) with references therein.

ELAs obtained by the AAR method (Table 2) are lower for G3 and G4 and have larger uncertainty intervals than the ELAs calculated with the AABR method. Yet, the relative difference in ELA between the reconstructed G3 and G4 remains roughly the same when comparing the results obtained by the two methods for calculating ELA. This is not the case for G1 due to the relatively flat valley floor on which the valley glacier propagated (Nesje 1992a, b; Benn & Lehmkuhl 2000). The calculated AABR ELAs of the glaciers G1, G3 and G4 are 134, 147 and 172 m above a corrected sea level, respectively.

Present and past depositional environment in lake Ner-Finnkongdalsvatnet

Lake Ner-Finnkongdalsvatnet is an elongated basin with a deeper (14 m) NW part and a shallow (2–4 m) SE part (Fig. 4). Only a small area near the centre of the basin is suitable for coring, due to the slope gradient (Dahl *et al.* 2003). The shallower SE basin, near the main inlet, has a smooth sediment surface that is gently sloping towards the NW. Nine cores were collected and analyses were carried out on four of them (Fig. 2 for coring sites). Seventeen samples were radiocarbon dated. Five radiocarbon dates were rejected from the age-depth model as they are probably resedimented older carbon or contaminated. The three dates Poz-48485, Poz-48487 and Poz-48488 were rejected from the age-depth model, as they apparently give too old ages. It is suggested that these dated plant remains have been remobilized due to reworking of sediments further upstream and then redeposited in the lake. The samples Poz-51778 and Poz-51779 are based on only 0.3 and 0.25 µg TOC and yield very young ages compared to other dated samples at the same depth intervals. These samples are rejected from the age-depth model as they are thought to be contaminated by modern carbon.

Based on the variability of the physical sediment properties, including LOI, DBD, grain-size, MS and geochemical properties, the lithology of the lake is divided into units A–K (Figs 5–7, Table 3). Except for unit K, all units are identified and correlated between the four cores from lake Ner-Finnkongdalsvatnet (Fig. 5).

The core-to-core correlation shows that individual sediment parameters from NFP 409 and NFP 809 generally correlate very well, with correlation coefficients ranging between 0.45 and 0.94, either positively or negatively (Table S1).

The measurement values of DBD, MS, Ti, Ca, K and Si are generally higher in core NFP 409 compared with the corresponding units in NFP 809 (Fig. 6).

Discussion

Geomorphology

The geomorphology in the drainage area of lake Ner-Finnkongdalsvatnet (Fig. 2) indicates four main sources of sediment influx. These are glacier meltwater, colluvial processes including debrisflows and snow avalanches, extra-glacial in-wash and *in situ* production/external input of organic material. As it may be possible to distinguish among these sediment sources based on mineralogical, chemical and biological characteristics, the lithology of lake Ner-Finnkongdalsvatnet cores is suggested to be well suited for studying the relative impact of glacier variations.

Timing of rock glacier formation and climatic implications. – The timing of rock glacier formation is not well constrained in Finnkongdalen. The interpreted rock glacier on the NE valley side of Finnkongdalen is located partly within the outline of the reconstructed glacier G1 and is partly overriding the M2 ice-marginal position (Figs 2, 4). This implies that rock glacier formation is younger than the formation of both the M1 and M2 glacier margin positions (Figs 2, 4). Given that the age of the interpreted till in unit K is bracketed between 21 970±620 and 14 300±330 cal. a BP, the position of

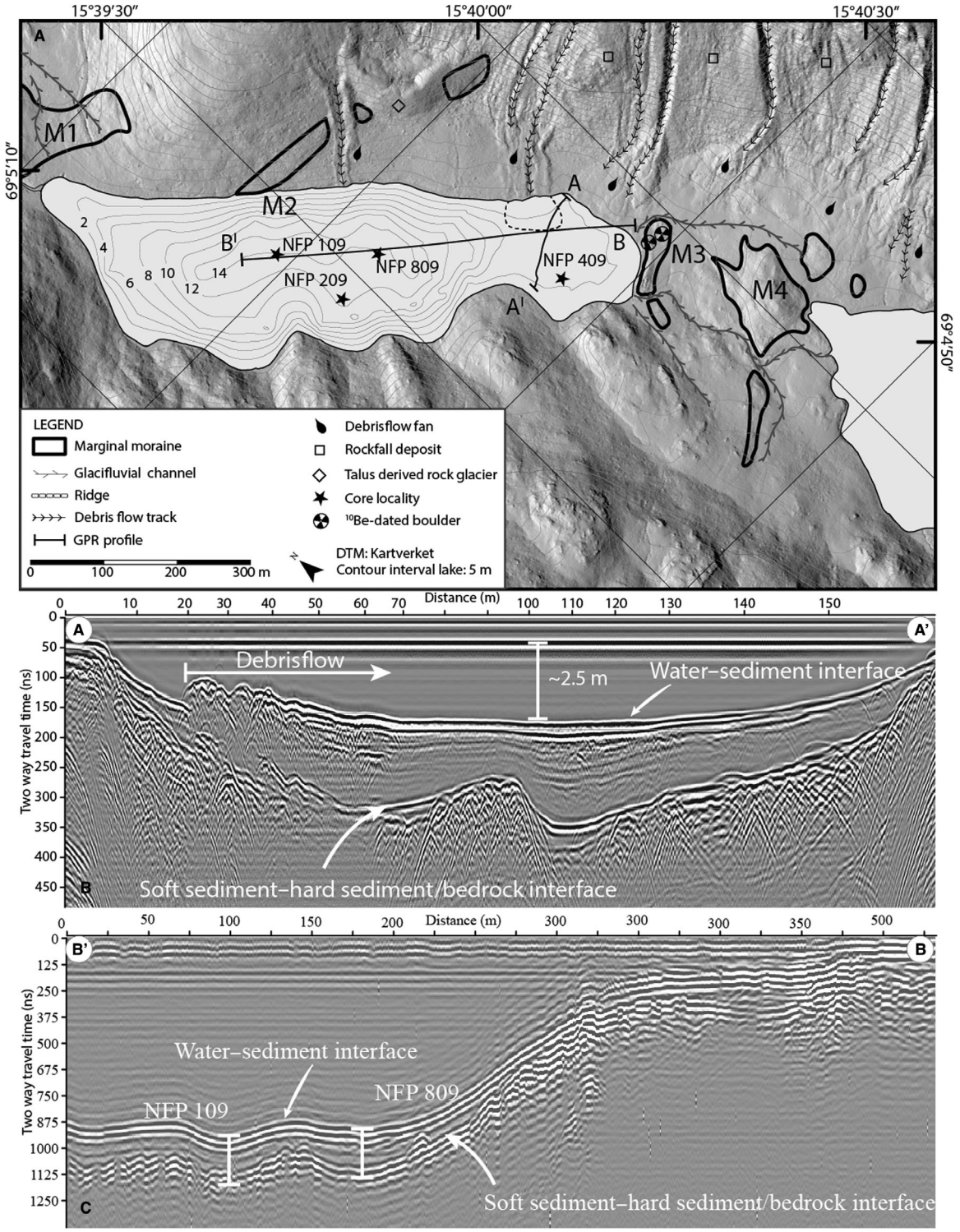

Fig. 4. A. Map of Ner-Finnkongdalsvatnet with emphasis on bathymetry, core localities and landforms related to glacial, periglacial (rock glacier) and slope processes in the area immediately surrounding the lake. Note that the primary source of glacially eroded sediments is relict meltwater channel inlets at the S-SE lake shore, while extra-glacial in-wash may be transported by surface runoff and small streams down the valley sides surrounding the lake, as well as by slope processes of larger magnitude along the SE valley side. B. GPR profile (100 MHz) showing reflectors indicating sediment surface, and the transition from possibly organic gyttja with high water content and minerogenic sediments/bedrock. The undulating sediment surface in the eastern part of the radargram indicates the surface of a debrisflow fan propagating 60–70 m into the lake from the E-NE valley side. C. GPR profile (25 MHz) showing reflectors indicating sediment surface, and the transition from possibly organic gyttja with high water content and minerogenic sediments/bedrock. Coring sites of NFP 109 and NFP 809 are marked on the radargram. Elevation data available from hoydedata.no (Kartverket 2022).

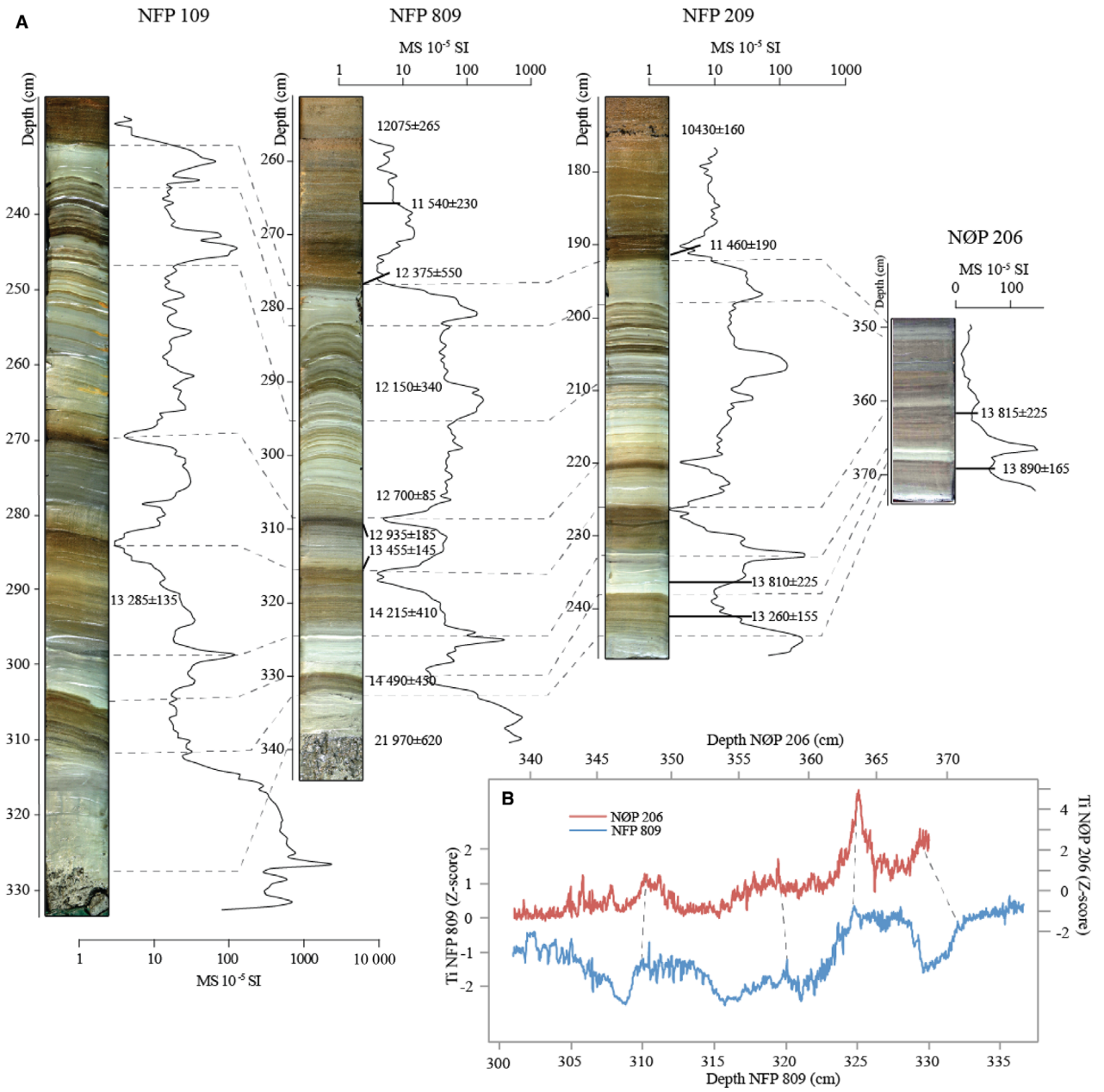

Fig. 5. A. Comparison of core imagery and MS in AMS ^{14}C-dated cores from Ner-Finnkongdalsvatnet (NFP) and Nøssdalsvatnet (NØP) further downstream. B. Comparison of highly resolved Ti (*Z*-score) between Ner-Finnkongdalsvatnet (blue line) and Nøssdalsvatnet (red line). Data from Nøssdalsvatnet are from Moe (2009).

the rock glacier implies that formation was initiated sometime after this time-span.

Rock glacier formation requires a dry to moderately humid climate with cool summers, and it has been shown that there are generally no significant differences in temperature, yet slightly drier conditions, on rock glaciers than on the ELA of nearby glaciers (Humlum 1998). Nearby talus-derived rock glaciers at Bleik, NW Andøya, became inactive about 15.7 ka (H. Linge, pers. comm. 2022). The melt-out of the rock glaciers at Bleik is in accordance with the indicated increase in regional air temperature on northern Andøya (Alm 1993), and is suggested to mark the end of continuous permafrost conditions near sea level on Andøya.

Glacier and ELA reconstruction. – Although the marginal moraines M1, M3 and M4 (Fig. 2) allow for very accurate reconstructions of the glacier fronts, there is no geomorphological evidence indicating the glacier surface profile further upvalley. To overcome this problem, the surface profiles of the glaciers G1, G3 and G4 were

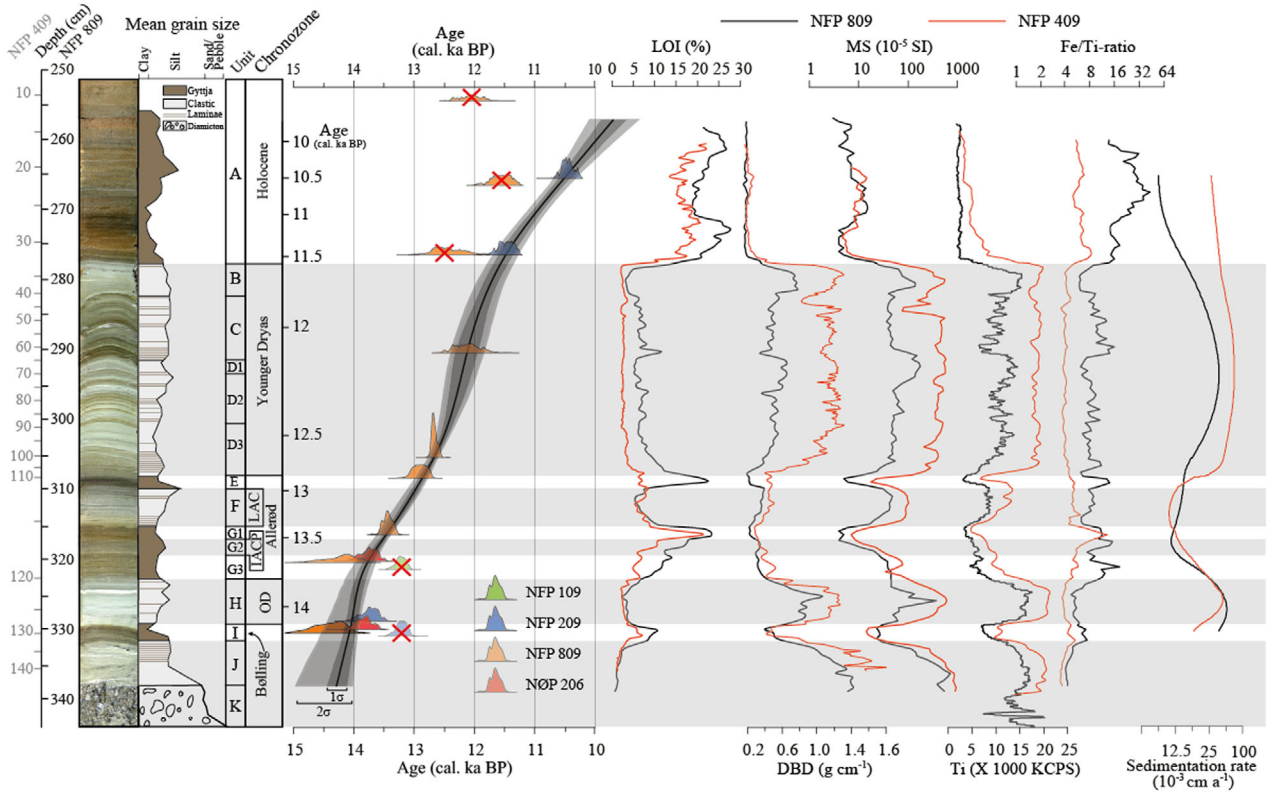

Fig. 6. Image and sediment log on the left side. The age-depth model on the left of the diagram is constructed using AMS ^{14}C-dated terrestrial plant macrofossils from NFP 109, 209, 809 and NØP 206. Age model is marked with a best-fit curve within a dark-shaded 1σ- and a light-shaded 2σ uncertainty band. Red crosses mark outliers that are rejected. LOI, DBD, MS, Ti count rate and the Fe/Ti ratio in sediments from NFP 809 (black curves) and NFP 409 (red curves) are plotted against the depth scale of NFP 809. A comparison of sedimentation rates in NFP 809 and 409 is shown on the right side of the diagram. Shaded areas are suggested periods of increased input of glacially derived minerogenic sediments to the lake. The depth scale of core NFP 409 is converted to the depth scale of NFP 809 for representation, based on correlation between core units presented in Fig. 5.

reconstructed using the steady-state model of Benn & Hulton (2010). This model calculates the ice-surface elevation along the central flowline, based on the relationship between the shear stress and rate of ice deformation, and by assuming a perfect ice plasticity with an ice density of 900 kg m^{-3} (Nye 1952; Schilling & Hollin 1981). The shear stress is here estimated to be 65 kPa by comparing modelled ice-surface gradients with the measured altitude and gradient of lateral moraines near the glacier front.

The AAR method is suitable when reconstructing ELAs on small and simple glacier systems (Osmaston 2005; Oien *et al.* 2021). The ELA based on AAR of G1 (168±13 m a.s.l.) is indistinguishable from that of G3 (166±10 m a.s.l.) (Table 2, Fig. 3). This effect is the result of the assumption that the AAR for valley and cirque glaciers is fixed, regardless of glacier hypsometry (Nesje 1992a, b; Benn & Lehmkuhl 2000). This is on the other hand less pronounced when the ELA is calculated with the AABR technique, as this calculation includes the BR based on a highly resolved elevation-area distribution (Osmaston 2005). The AABR technique is thus generally the more reliable of the two techniques when reconstructing past changes in the ELA of former valley glaciers propagating along a gently sloping valley floor (Table 4).

Interpretation of lithology

Glacial and extra-glacial in-wash. – The correlation and PCA analyses (Table S1, Fig. 8) confirm that the sediment variables can be divided into two groups, with an organic rich sediment type on one side (LOI and Fe/Ti ratio) and a more minerogenic sediment type on the other side (DBD, MS, Ti, Si, Ca and K). The PCA 1 axis explains 89.2 and 80.3% of the variability in the included parameters from NFP 409 and NFP 809, respectively. The variability in MS and Fe, and to some extent in Si, is less influenced by the clastic content relative to the parameters DBD, Ti, K, Ca and the inversely correlated parameters LOI and Fe/Ti ratio. The DBD, and count rates of Ti, Ca and K are therefore found to be suitable proxies for the input of clastic sediments to Ner-Finnkongdalsvatnet.

The Fe/Ti ratio is commonly associated with redox related processes, and an elevated Fe/Ti ratio may

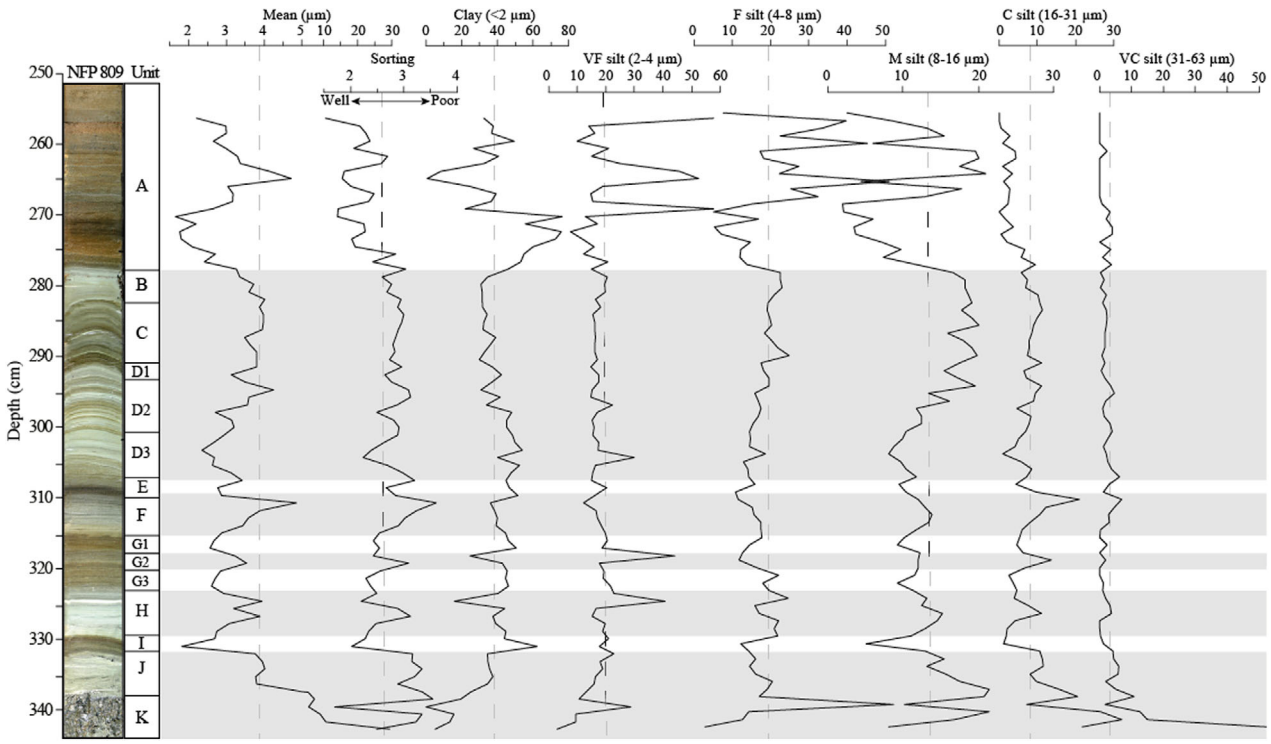

Fig. 7. Grain-size parameters from NFP 809. Shaded areas are suggested periods of increased input of glacially derived minerogenic sediments to the depositional environment in the lake.

indicate an oxic depositional environment (Croudace *et al*. 2006). As the Fe/Ti ratio correlates well with LOI and inversely with the minerogenic indicators DBD, Si, Ca and K, it is inferred that variations in the Fe/Ti ratio mainly mirror remobilization and in-wash of previously subaerially exposed sediments of mainly extra-glacial origin.

Based on the mapped geomorphology (Fig. 2), it is likely that glacial activity and colluvial processes are the major contributors to the clastic sediment input in Ner-Finnkongdalsvatnet. Typical distal sedimentological indicators of debris flows or other processes involving rapid remobilization and redeposition in high-energy depositional systems are erosional contacts, upward-fining facies and elevated Fe/Ti ratio. There is a possibility that layers of elevated organic content and Fe/Ti ratio throughout the lithology may represent mass-wasting events. Still, no erosional contacts nor upward-fining facies typically related to mass-wasting turbidites are observed within the investigated lithology. Sediments related to the interpreted debris flow fan propagating into the lake are not identified in the sampled lithology. It is thus likely that this debris flow fan was most active during the Holocene. This is in accordance with a study from Langøya, 60 km southwest of the study showing an intensification in debris flow activity during the latter part of the Holocene (Nielsen *et al*. 2016b). Furthermore, Vasskog *et al*. (2011) argue that most of their records of mass-wasting events show an increasing tend throughout the Holocene.

It is suggested that the variability in Ti mainly reflects a balance of influx of glacially eroded clastic sediments relative to the input of extra-glacial in-wash and *in situ* production/external input of organic material. This depositional balance is affected by change in one process relative to the sum of processes. Quantification of each depositional process is dependent on the ability to quantify all depositional processes. The sediment budget related to glacial processes is normally much bigger than those associated with in-wash in settings with a low catchment- to glacier-area ratio (e.g. Dahl *et al*. 2003). Hence, in the current setting, it is likely that glacially eroded sediments dominate the influx of clastic sediments to Ner-Finnkongdalsvatnet during periods of extensive glacier activity in the upper part of Finnkongdalen valley.

The Ti-count rate in units B, C and D in NFP 409 remains high and relatively stable in contrast to the corresponding units in NFP 809 (Fig. 6). In addition, the sedimentation rate is systematically higher in those units that are suggested to mainly consist of subglacially eroded material (units B, C, D and H) in NFP 409 than the corresponding units in NFP 809. Thus, we argue that the variability in Ti in NFP 409 may be a suitable proxy of small-scale changes in glacier size when the glacier extent is relatively small, whereas the Ti-count rate in NFP 809

Table 3. Lithological observations and interpretation.

Observations	Interpretation
Unit K (346.9–338.0 cm/>14 300±330 cal. a BP) Matrix-supported diamicton with grain sizes ranging from clay to cobbles. The measured grain-size percentages of the matrix indicate that the matrix generally consists of very fine to fine silt, as these two grain-size classes amount to 81%. Visually inspected clasts are generally subrounded to more angular, but well-rounded clasts occur. Due to sampling difficulties, other sediment properties could not be measured, and results from both MS and XRF scanning are unreliable because of a very rough sediment surface. A single *polytrichum* leaf was observed incorporated in matrix material.	Sediments are interpreted as till. Coring site of NFP 809 and 109 was overrun by a glacier, depositing the interpreted till (Fig. 4).
Unit J (338.0–331.6 cm/14 300±330–14 130±210 cal. a BP) Upward-fining sandy silt. Ti, Si, K and Ca counts, as well as DBD are high with low variability in the upper part of the unit, while more variability occurs near the base. Several fractions of very coarse sand to fine gravel are present in the lower part of the unit. The transition to the unit below is abrupt. An upward-fining sequence of 2 cm is observed at the base of the unit. This unit is 17 cm thick in core NFP 109 and only 6 cm thick in core NFP 809 (Fig. 5A).	Sorted minerogenic sediments are interpreted as water-lain sediments in a glaciolacustrine depositional environment. This implies that the transition between units K–J represents the deglaciation of the coring site of NFP 809. The thicker unit in NFP 109 is suggested to indicate that deglaciation and thus the onset of glaciolacustrine deposition took place earlier at the coring site of NFP 109 than at NFP 809 (Figs 4A, 5A).
Unit I (331.6–329.4 cm/14 070±180–14 130±210 cal. a BP) Organic-rich clayey gyttja. LOI rises to 7.0 and 10.5% in NFP 409 and NFP 809, respectively. The Fe/Ti ratio is relatively variable with slightly increased values in two layers at 329.9–329.4 and 331.6–330.7 cm. The transitions in both ends are abrupt and characterized by an increase in Ti, Si, K and Ca counts, as well as DBD across the upper and a decrease across the lower boundary.	The organic-rich clayey gyttja indicates that the depositional environment is less dominated by minerogenic input and there is increased relative importance of extra-glacial in-wash and *in situ* production/external input of organic material. The sediments are interpreted to indicate a significant retreat of the glacier front, possibly proximal to lake Øver-Finnkongdalsvatn.
Unit H (329.4–322.7 cm/14 070±180–13 910±140 cal. a BP), Clayey silt with high Ti, Si, K and Ca counts, as well as DBD. Organic content is low (LOI: 1–2%). The Fe/Ti ratio remains low with relatively little variability throughout the unit. A characteristic light grey layer consisting of well-sorted very fine to fine silt is present at 325.2–324.6 cm. A corresponding layer is observed in all cores collected from the lake, as well as in NØP 206 collected from the downstream Nøssdalsvatnet (Figs 1, 4, 5). The thickness of the layer is similar in all cores.	The clayey silt, along with low organic content, indicates that the depositional environment is dominated by clastic input and that extra-glacial in-wash and *in situ* production/external input of organic material is very low. The unit is interpreted to represent glacier advance. Light grey layer of very fine to fine silt in the upper part of the unit is interpreted as a loess deposit (see Discussion).
Unit G (322.7–315.0 cm/13 910±140–13 360±90 cal. a BP) Silty gyttja with high organic content (LOI: >20%) and lower DBD values, as well as lower Ti, Si, K and Ca counts. The Fe/Ti ratio rises significantly in NFP 409, while the corresponding rise in NFP 809 is less significant. Two separate layers with somewhat higher Ti, Si, K and Ca counts, as well as DBD, as well as lower LOI values, occur in the middle part of the unit. Unit G is therefore subdivided into the three subunits G1, G2 and G3, where subunit G2 has somewhat higher values for minerogenic input and lower LOI than subunits G1 and G3.	The organic rich silty gyttja is indicative of a depositional environment less dominated by minerogenic input and increased relative importance of extra-glacial in-wash and *in situ* production/external input of organic material. The unit is interpreted to represent less influx of glacifluvially transported glacigenic sediment to the lake, indicating a significant retreat of the glacier front. Subunit G2 is interpreted as an increase in influx of glacigenic sediments to the lake, caused by a glacier advance. Subunit G1 shows many of the same sedimentological characteristics as unit A (Holocene), with no indications of glacigenic sediment influx and high indicators of extra-glacial in-wash and *in situ* production/external input of organic material. It is therefore interpreted that the glacier was absent from the catchment when subunit G1 was deposited.
Unit F (315.0–309.4 cm/13 360±90–12 945±70 cal. a BP) Upwards coarsening clayey silt with increased levels of coarse silt upward. Organic content is generally low (LOI: <10%) and decreasing upward.	In general, the clayey silt indicates increased influx of glacigenic clastic sediments to the lake and that the relative importance of extra-glacial in-wash and *in situ* organic production is low. It is interpreted that the base of the unit represents glacier re-formation. The upward coarsening indicates increased hydrological energy and may indicate increasing glacifluvial runoff, probably due to increasing glacier size.
Unit E (309.4–307.8 cm/12 945±70–12 835±65 cal. a BP) Organic rich clayey gyttja (LOI: >20%). Significant and abrupt decrease in Ti, Si, K and Ca counts, as well as DBD at the base of the unit.	The organic rich clayey gyttja has no indications of glacigenic sediment influx and high indicators of extra-glacial in-wash and *in situ* production/external input of organic material. It is therefore interpreted that the glacier was absent from the catchment when unit E was deposited.

(continued)

Table 3. (continued)

Observations	Interpretation
Unit D (307.8–290.8 cm/12 835±65–12 140±235 cal. a BP) Upward coarsening clayey silt. There is a relatively high variability of Ti, Si, K and Ca counts and the Fe/Ti ratio. Organic content is generally low, yet with some variation (LOI: 6–12%). Upward coarsening by increased levels of medium silt upward throughout the unit. Based on the variability of Ti, Si, K and Ca counts, as well as DBD and organic content, Unit D is subdivided into the three subunits D3, D2 and D1, where subunit D2 has somewhat lower values for minerogenic input and higher LOI than subunits D3 and D1.	The clayey silt indicates increased influx of glacigenic clastic sediments to the lake and that the relative importance of extra-glacial in-wash and *in situ* production/external input of organic material is lower than unit E below. It is interpreted that the base of the unit represents glacier re-formation. The upward coarsening indicates increased hydrological energy and may indicate increasing glacifluvial runoff, probably due to increasing glacier size.
Unit C (290.8–281.9 cm/12 140±235–11 810±220 cal. a BP) Clayey silt with upward decreasing organic content. The base of the unit is marked by increased level of organic content (LOI: 9%). Higher variability of LOI and Fe/Ti ratio compared with unit D below and B above is observed.	The variability in organic content and Fe/Ti ratio is indicative of a varying relative importance of influx of glacifluvially glacigenic sediments on one hand and extra-glacial in-wash and *in situ* production/external input of organic material on the other. The general upward decrease in organic content indicates a relative increased importance of extra-glacial in-wash and *in situ* production/external input of organic material. The cause of the observed variability is interpreted as either temporal variations of glacifluvial runoff or temporal variations in extra-glacial runoff.
Unit B (281.9–279.1 cm/11 810±220–11 645±200 cal. a BP) Upward-fining clayey silt with low organic content (2–3%). The base of the unit is marked by an increase in Ti, Si, K and Ca counts, as well as DBD, a slight lowering in organic content and a lower Fe/Ti ratio.	The clayey silt and low organic content indicate domination of influx of glacifluvially glacigenic sediments into the lake.
Unit A (<279.1 cm/>11 645±200 cal. a BP) Clayey/silty gyttja. High organic content (LOI: >13–26%) and elevated Fe/Ti ratio.	The organic rich clayey gyttja has no indications of glacigenic sediment influx and high indicators of extra-glacial in-wash and *in situ* production/external input of organic material. It is therefore interpreted that the base of the unit marks the final demise of the glacier in the catchment.

is better suited for reconstructing glacier size in periods when the glacier was relatively large.

Continuous glacier reconstruction. – The interpretation of glacial history in the catchment is based principally on the ^{14}C-dated Ti record from NFP 809. The Ti (*Z*-score) is the basic key to glacial extent over the period 14 300±330–11 645±200 cal. a BP, with high *Z*-scores indication large glacier area. The moraine ^{10}Be ages are consistent, yet they do not tightly constrain timing of moraine formation. The ^{10}Be dates indicate that the formation of the moraine M3 occurred within the time interval 14.5–11.1 ka (Fig. 9A, Table 1). Moraine ridges, such as M3, are susceptible to postdepositional reworking due to e.g. melt-out of glacier ice, periglacial processes or fluvial erosion. In such cases, cosmogenic dating methods are vulnerable to yielding too young exposure ages. On the contrary, a complex history of remobilization and redeposition of boulders may yield too old ages. Thus, the ^{10}Be dates do not indicate the age of moraine formation precisely, nor rule out any of the glacier advances interpreted from the lithology in lake Ner-Finnkongdalsvatnet (Figs 9A, 10). Based on the position of M4 relative to the ^{10}Be-dated M3 as well as the radiocarbon-dated lake sediments, it is suggested that the formation of M3 most likely took place around 14 000 cal. a BP, while M4 was formed close to the end of the Younger Dryas (YD), after about 11 800 cal. a BP. The ^{10}Be dates are also consistent with an alternative interpretation that M3 was formed during Bølling and M4 during the OD. This interpretation is, however, regarded as less likely as there are no moraines observed upvalley from M4 and the Ti (*Z*-score) clearly indicates the presence of glacier activity during the YD. It is suggested that the glacier was completely melted away after about 11 500 cal. a BP. These interpretations are key to the continuously reconstructed ELA and thus also winter precipitation reconstruction. Due to the large uncertainty intervals of the ^{10}Be ages and the fact that M4 is not dated directly, there is some degree of uncertainty to the actual age of moraine formation.

From the stratigraphy in Ner-Finnkongdalsvatnet it is suggested that the glacier melted away completely and re-formed on three occasions during the interval between the deglaciation of the lake 14 300±330 cal. a BP and the final deglaciation of the catchment after 11 645±200 cal. a BP. DBD, Ti, Si, Ca and K indicate that the glacier advanced during the OD (14 070±180–13 910±140 cal. a BP) and YD (12 855±65–11 645±200 cal. a BP) were more extensive than the advances during the Intra Allerød Cold Period (IACP; 13 820±70–13 530±95 cal. a BP) and Late Allerød Cooling (LAC; 13 360±90–12 945±70 cal. a BP). Smaller glacier advances are suggested to have taken place within the YD, the latter being the largest.

Table 4. Radiocarbon ages from the different cores in the catchment. Dated material is sampled from four different cores and calibrated using the IntCal20 calibration curve in clam v 2.4.0. (Blaauw 2010; Reimer *et al.* 2020).

Core	Depth[1] (cm)	Lab. no.	Sample type	^{14}C age	Calibrated age (2σ cal. a BP)	Area under probability curve (2σ)	Depth[2] (cm)
NFP 109	291–292	Poz 51779	Plant macrofossils	11 380±80	13 285±135	0.91	320–321
NFP 209	174–175	Poz 51775	Plant macrofossils	9290±60	10 430±160	0.91	265–266
	190–191	Poz 51776	Plant macrofossils	10 000±50	11 460±190	0.88	276–277
	236–237	Poz 51777	*Polytrichum* leaves	11 900±110	13 810±225	0.92	328–329
	239–241.5	Poz 51778	*Polytrichum* leaves	11 360±90	13 260±155	0.95	331–332
NFP 809	254–255	Poz 48485	Plant macrofossils	10 280±80	12 075±265	0.78	254–255
	266–267	Poz 48487	*Polytrichum* bud	10 040±70	11 540±230	0.89	266–267
	276–277	Poz 48488	Plant macrofossils	10 600±210	12 375±550	0.95	276–277
	289–292	Poz 48489	Plant macrofossils	10 310±100	12 150±340	0.91	289–292
	305–306	Poz 48490	Plant macrofossils	10 740±70	12 700±85	0.92	305–306
	308–309	Poz 48491	Plant macrofossils	11 030±130	12 935±185	0.93	308–309
	316–317	Poz 48492	Plant macrofossils	11 610±80	13 455±145	0.95	316–317
	321–322	Poz 48493	Plant macrofossils	12 220±130	14 215±410	0.83	321–322
	329–332	Poz 48494	Plant macrofossils	12 320±120	14 490±450	0.95	329–332
	338	Poz 48495	*Polytrichum* leaf	18 170±250	21 970±620	0.95	336–338
NØP 206	360.5	Poz 29135	Plant macrofossils	11 910±110	13 815±225	0.92	320–321
	368.5	Poz 29136	Plant macrofossils	11 970±100	13 890±165	0.80	330–331

[1]Sample depths referring to the host core.
[2]Sample depth is recalculated to the master depth scale of NFP 809.

Furthermore, the low sedimentation rates in the lithological units corresponding with the IACP and LAC re-formations relative to the units related to the OD and YD re-formations (Fig. 6), may indicate that glacigenic input was reduced due to the presence of a significant upper lake. It is suggested that the glacially eroded sediments were most likely deposited directly into Ner-Finnkongdalsvatnet during the OD and YD glacier advances.

As a result of a sudden shift to a warmer climate, the regional ELA rose rapidly by several hundred metres following the YD period (Vorren *et al.* 1988; Alm & Willassen 1993; Paasche *et al.* 2007; Aarnes *et al.* 2012; Birks *et al.* 2012, 2014). It is therefore likely that Unit A, dated to <11 645±200 cal. a BP, represents a fully deglaciated catchment. Sediment properties similar to those dated <11 645±200 cal. a BP are thus used as indicators of a deglaciated catchment.

The continuously reconstructed local ELA (Fig. 10) is based on a linear regression between the record of Ti counts and the calculated local ELA of G3 and G4, as well as the minimum ELA required for glacier formation within the catchment, in effect the elevation of the top of the backwall (370 m above present sea level) (Fig. 9B). This relationship is in other words apparently linear with the number of data points available ($n = 3$). Considering the low number of data points linking the records ($n = 3$), there is a possibility that the true relationship does not have a linear nature. This represents a source of error that is not possible to account for in more detail. There is a higher level of uncertainty for higher ELA predictions, considering that the flux of glacigenic sediment into the lower lake would fall drastically as soon as the glacier receded enough to expose the upper lake Øver-Finnkongdalsvatnet. This effect is not possible to resolve from our data and is therefore not quantified or accounted for.

Variations in mean annual winter precipitation as snow

In addition to providing a record of glacial activity, the lithological evidence can be used to infer winter precipitation as snow at the ELA by combining the ELA record with an independent reconstruction of ablation season temperature, by using the Liestøl relationship (e.g. Liestøl 1967; Lie & Paasche 2006). Regional winter precipitation as snow (Fig. 10D) is inferred by converting the T_{Jul} record (Fig. 10B) to summer temperature (Fig. 10C), using a modern analogue. The summer temperature record is corrected for an aspect related temperature lowering of −1.95±0.325 °C. Next, the summer temperature reconstruction (Fig. 10C) is corrected for the effect of altitudinal changes on temperature, using an altitude lapse rate of −0.65 °C 100 m^{-1}, which is close to the moist-adiabatic lapse rate found to be realistic during the summer-half of the year (Engen-Skaugen & Tveito 2007). Lastly, the regional winter precipitation (Fig. 10D) is inferred by correcting the winter balance at the ELA for a D/A ratio of 3.83.

Each step of the workflow presented above is included to make as precise estimates as possible given the data set provided. Yet, there are a number of potential sources of error associated with the workflow. Many of these are not possible to quantify and the identified error sources are difficult to validate. The shaded areas representing uncertainty in the diagrams in Figs 10 and 11 are the uncertainty surrounding T_{Jul} from Lusvatnet (Birks *et al.* 2014), ELA reconstruction, the inferred uncer-

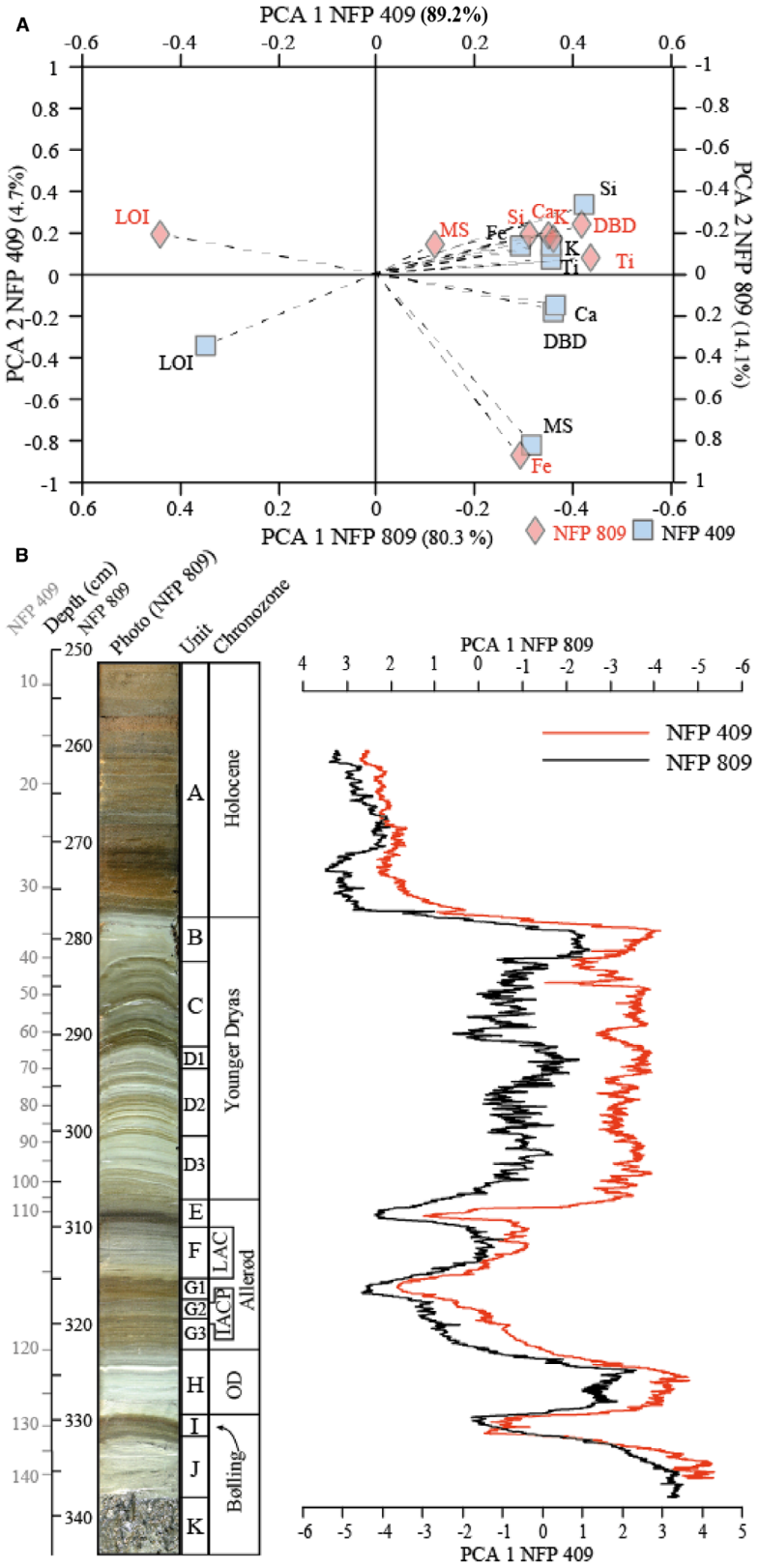

Fig. 8. A. PCA scores of LOI, DBD, MS, Ti, Fe, Ca, K and Si in both NFP 809 and 409 are plotted against the PCA 1 and PCA 2 axes. Together, these axes explain 93.9 and 94.4% of the variability in NFP 409 and NFP 809, respectively. B. PCA 1 of NFP 809 (black) and NFP 409 (red) plotted against the depth scale of NFP 809.

tainty associated with the relationship between the reconstructed ELA record and the Ti *Z*-score record from the core lithology and uncertainty around the effect of valley aspect on temperature and the modern relationship between July temperature and ablation season temperature.

Independent proxy for ablation season temperature. – Because Andøya is situated close to the Norwegian shelf break (Fig. 1), it remained mostly ice-free during the Lateglacial (Andersen 1975; Rasmussen 1984; Møller *et al.* 1992; Vorren & Plassen 2002; Vorren *et al.* 2015). A number of continuous quantitative terrestrial palaeoenvironmental reconstructions from Andøya are available (Alm 1993; Alm & Willassen 1993; Vorren *et al.* 2009, 2013; Aarnes *et al.* 2012; Birks *et al.* 2014; Alsos *et al.* 2020).

Past variations in solid mean annual winter precipitation are quantified based on the continuous reconstructed local ELA during the deglaciation in Finnkongdalen and mean ablation season temperatures recalculated from a continuous T_{Jul} record from Lusvatnet ~3 km SW of Finnkongdalen (Fig. 1; Birks *et al.* 2014). Three T_{Jul} records, based on pollen, chironomids and plant macrofossils, respectively, have been reconstructed from Lusvatnet. In addition to air temperature, chironomids respond to changes in water temperature (Birks *et al.* 2000), and hence to fluctuations of the local glacier situated in the Lusvatnet catchment during parts of the Lateglacial (J. Bakke, pers. comm. 2022). Despite lower uncertainty presented for the chironomid-assemblage method used in Lusvatnet, and too sparsely distributed terrestrial plant macrofossils, the pollen-based reconstruction is suggested to be the most representative continuous record of T_{Jul} from Lusvatnet (Fig. 10B). Corrections of the Lusvatnet T_{Jul} record are necessary before applying it to the Liestøl equation. These are explained in the following paragraphs. This record extends back to only ~13 600 cal. a BP, so the data does not provide basis for winter precipitation for the early part of the core record in Ner-Finnkongdalsvatnet.

Historical temperature data from Andenes, 30 km north of Finnkongdalen, show that mean ablation season temperature (1st May–30th September) is currently on average 2.3±1 °C lower than mean July temperature (n = 118 from meteorological station 87100 between AD 1900 and 2021; MET 2021). This present relationship between mean July and mean ablation season temperature is assumed for the precipitation reconstruction in Fig. 10D. The effect of increased seasonality with increased summer solar radiation to the Northern Hemisphere during the latter part of the Lateglacial is not accounted for (Kutzbach *et al.* 2008), and the inferred ablation season temperature may thus be slightly overestimated.

Owing to the N-NW orientation of Finnkongdalen valley, the T_{Jul} record of Lusvatnet is suggested to be too warm for direct comparison. Based on modern glaciers in Troms, northern Norway, Andersen (1968) estimated an ELA difference between north- and southwards facing cirque glaciers of 250–350 m due to differences in insolation. As the aspect of Finnkongdalen is 325° NW, the mean ablation season temperature used in the Liestøl equation is therefore adjusted for an effective aspect-related ELA lowering of 300±50 m, resulting in insolation-related temperature lowering of −1.95±0.325 °C when an altitude lapse rate of −0.65 °C 100 m^{-1} is applied.

Wind-transported snow may have a significant effect on the local temperature-precipitation-wind ELA (TPW-ELA) of cirque and valley glaciers compared to the more regional impact of solid winter precipitation on the temperature-precipitation ELA (TP-ELA) of ice caps (Dahl & Nesje 1992, 1996; Nesje & Dahl 2003).

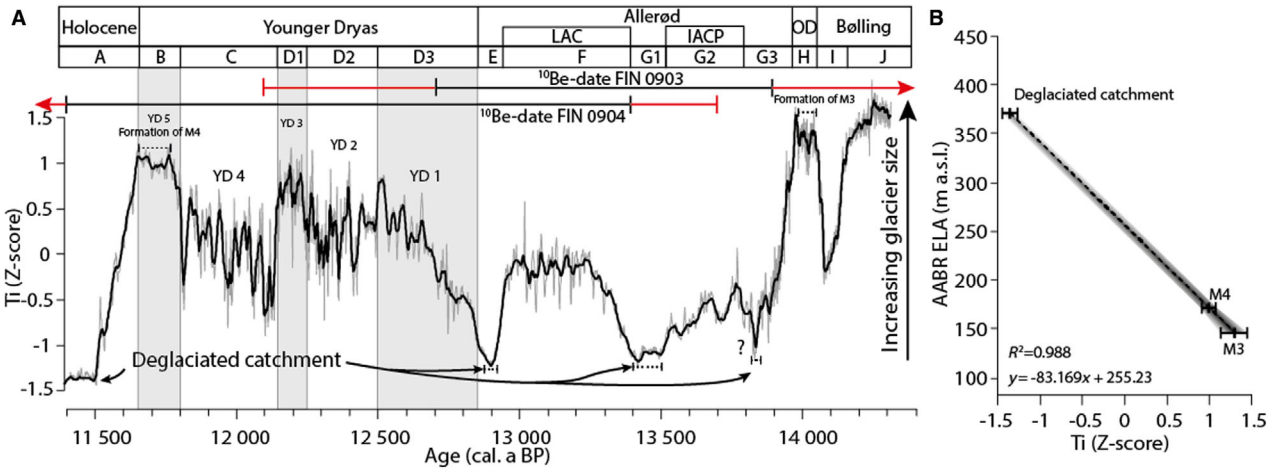

Fig. 9. A. Ti count rate (15 point running mean *Z*-score) plotted against modelled age. Age intervals of the ^{10}Be dates of M3 and M4 are presented along the age-axis. B. Linear regression between reconstructed ELAs based on moraines (Table 2) and the average Ti count rate (*Z*-score) during periods of suggested moraine formation.

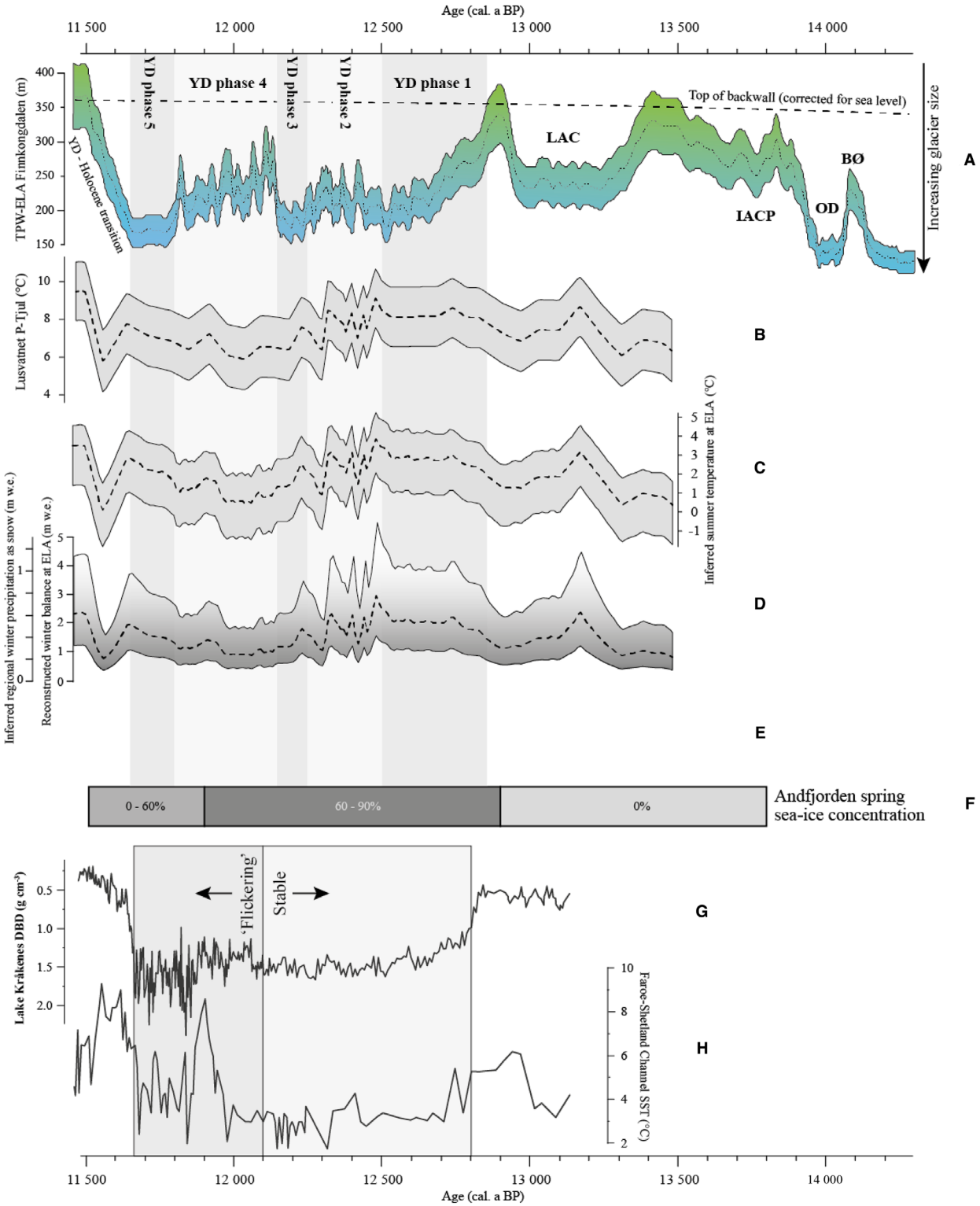

Fig. 10. A. Continuously reconstructed local ELA at Finnkongdalen between 14 300±330–11 645±200 cal. a BP. B. Pollen based July temperature reconstruction from Lusvatnet (Birks *et al.* 2014). C. Inferred mean ablation season temperature at Lusvatnet, following the procedure described in Paasche *et al.* (2007). D. Reconstructed mean annual winter precipitation as snow in Finnkongdalen based on the Liestøl equation. Minimum annual snowfall is indicated on the curve with a D/A ratio of 3.83 (see Dahl *et al.* 1997 for procedure). E. SST record from Andfjorden (Ebbesen & Hald 2004). F. Spring sea-ice concentration based on biomarkers reflecting the presence of sea-ice diatoms (Cabedo-Sanz *et al.* 2013). G. DBD values from Lake Kråkenes, situated in southwestern Norway. The DBD is viewed as a measure of glacigenic sediments released to the lake (Bakke *et al.* 2009). H. SST record from the Faroe-Shetland Channel in the northwestern North Sea (Bakke *et al.* 2009).

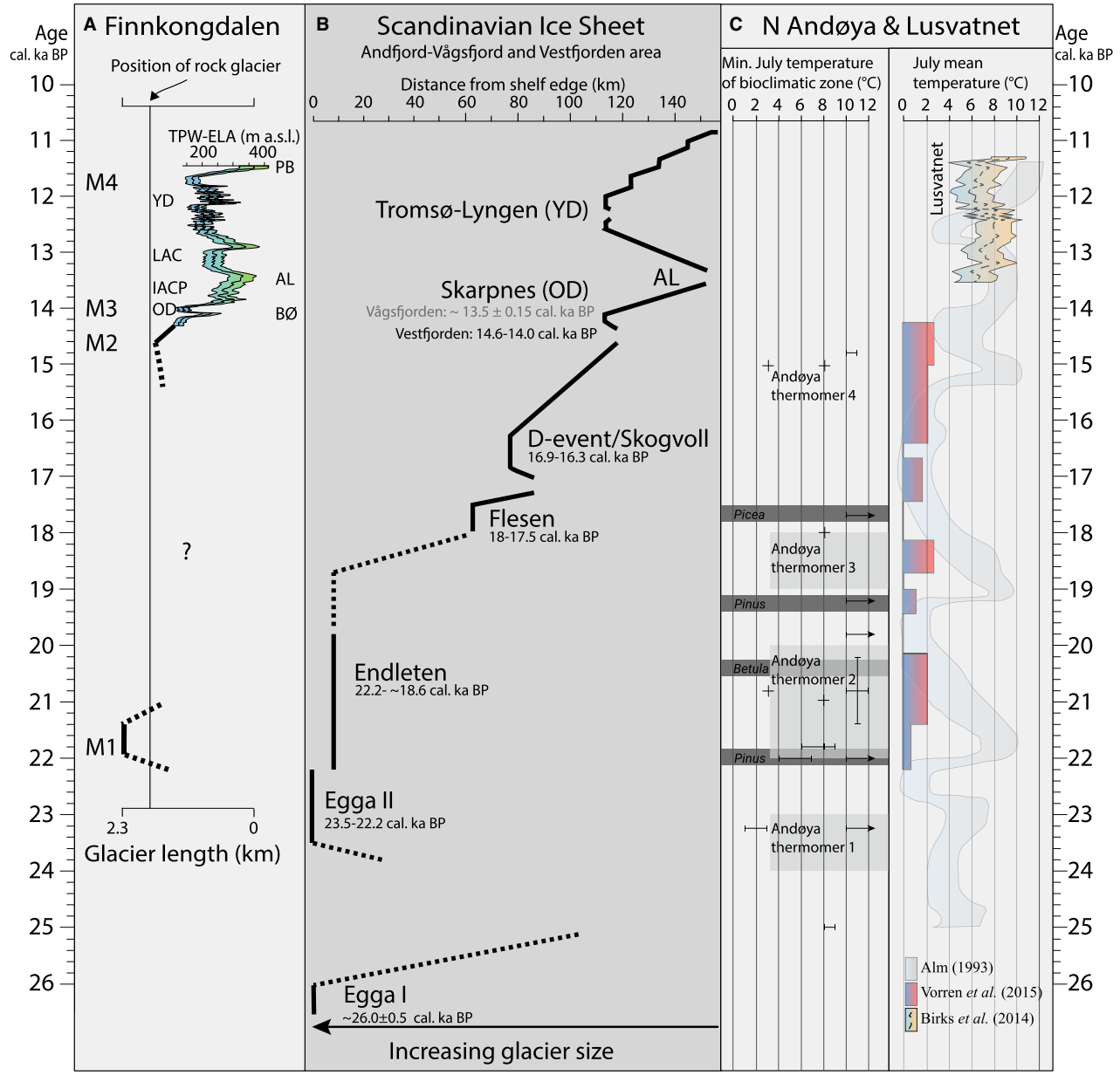

Fig. 11. Comparison between (A) reconstructed glacier fluctuations as reflected in glacier length and ELA in Finnkongdalen, (B) variations of the NW sector of the SIS during the Lateglacial (Vorren & Elvsborg 1979; Vorren & Plassen 2002; Dahlgren & Vorren 2003; Rørvik *et al.* 2010; Rydningen *et al.* 2013; Vorren *et al.* 2013, 2015; Laberg *et al.* 2018) and (C) presence of trees (Kullman 2006; Parducci *et al.* 2012), temperature reconstructions and inferred minimum July mean temperature of bioclimatic zone from northern Andøya and Lusvatnet (Fig. 1) (Fjellberg 1978; Vorren 1978; Alm & Birks 1991; Alm 1993; Elverland & Alm 2012; Birks *et al.* 2014; Vorren *et al.* 2015; Alsos *et al.* 2020).

Hence, the Liestøl equation cannot be used to validate the existence of small cirque and valley glaciers during the deglaciation in Finnkongdalen based on climatic inferences from temperature reconstructions and a theoretical depression of the regional TP-ELA alone.

Glacier fluctuations during the Lateglacial and climatic inferences

LGM–Bølling (units K–J). – The timing of the two glacier advances indicated by the M1 and M2 glacier positions is not dated directly. However, a *Polytrichum* leaf macrofossil found in the interpreted till matrix (unit K) dated to 21 970±620 cal. a BP indicates that Ner-Finnkongdalsvatnet was deglaciated just before or during the LGM (Figs 5, 11). This is in accordance with a ^{14}C-dated fragment of the bivalve *Mya truncata* found on Bleik, which reveals that parts of NW Andøya was ice-free at 21970±615 cal. a BP (Møller *et al.* 1992). The interpreted till in unit K may thus represent a major glacier advance corresponding with the Endleten event, reported by Rydningen *et al.* (2013) and Vorren

et al. (2013, 2015) (22.2 to ~18.6 cal. ka BP) (Fig. 11). Although no erosional contacts nor any signs of hiatuses were found in unit K, a complex depositional and erosional history of the till cannot be ruled out. Based on the morphostratigraphical position of the rock glacier, it is nevertheless likely that the glacier front remained proximal to the rock glacier after the deposition of the interpreted till in unit K, and that the glacier front overran the core site of NFP 809 (Figs 2–4) some time before 14 300±330 cal. a BP. The suggested LGM till in unit K is overlain by unit J, which consists of pebbles incorporated in graded glaciolacustrine sediments representing the retreat of the G2 glacier and the commencement of continuous glaciolacustrine sedimentation in the lake.

According to Paasche *et al.* (2007), two cirque glacier advances may have occurred on SE Andøya during the LGM (21 050–19 100 cal. a BP) and Heinrich Event 1 (H1) (17 500–14 700 cal. a BP), while the cirque was completely deglaciated after the early Bølling/Allerød warming (*c.* 14 700 cal. a BP) and throughout the YD. Their conclusions are in disagreement with the findings in this study. One explanation may be that the different glaciation history of the two cirques is due to differences in orientation and the slight elevation difference. However, the glacier variability of Paasche *et al.* (2007) is not dated directly, as the AMS ^{14}C-dated chronology is extrapolated beyond the oldest date of 13 100±90 cal. a BP. More research is needed to establish a regionally representative record of glacier fluctuation for the LGM and early Lateglacial.

Bølling (unit I) – glacier retreat. – Above unit J, sediments with a marked increase in LOI and distinct drops in DBD, MS and Ti represent unit I (Figs 6–8). The organic-rich sediments are dated to 14 070±180–14 130±210 cal. a BP, which is within the Bølling chronozone (Mangerud & Berglund 1978). The input of glacigenic material was dramatically reduced. Unit I was deposited over a few hundred years, and it is likely that the depositional environment in Ner-Finnkongdalsvatnet was strongly influenced by paraglacial activity within the recently deglaciated catchment. Indicators of minerogenic input are somewhat elevated compared with units A, E and G1, representing the Holocene and Allerød chronozones, respectively. Glacier activity can therefore not be ruled out. It is, however, likely that the glacier was small and that the input of glacigenic sediments to lake Ner-Finnkongdalsvatnet was reduced because of sediment trapping in lake Øver-Finnkongdalsvatnet.

Older Dryas (unit H) – short-lived glacier re-formation. – Unit H is dated to 14 070±180–13 910±140 cal. a BP within the OD and is suggested to represent the most pronounced glacial re-formation during the deglaciation in Finnkongdalen valley. A similar glacier event of suggested OD age has been described from the region (Rasmussen 1984). This corresponds well with recent results from Arnøy, 200 km NE of Andøya, showing that the local glaciers were larger during the OD than during the YD (Wittmeier *et al.* 2020). Adjusted for a land-uplift of about 25 m (Rasmussen 1984; Vorren *et al.* 1988; Møller 1989), the ELA reconstruction indicates a drop in the local TPW-ELA of about 120 to 147 m at the onset of the OD glacier re-formation/advance.

Except for cores retrieved near the main inlet, a distinct ~0.5-cm-thick layer of well-sorted, very fine to fine silt is found in the upper part of unit H in all cores from Ner-Finnkongdalsvatnet. A similar layer with the same characteristics, and in the same stratigraphical position, is also found in the downstream Nøssdalsvatnet (Figs 5, 7) where it is dated to approximately 13 975±90 cal. a BP (Moe 2009). These two layers share many of the same characteristics, including stratigraphical position in both Ner-Finnkongdalsvatnet and Nøssdalsvatnet. Even though the sedimentation rates above and below the layer are higher in Ner-Finnkongdalsvatnet, the layer has roughly the same thickness in both lakes. It is therefore likely that the very fine to fine silt in this layer has a different source than glacial meltwater streams from Finnkongdalen. Although more research is required, it is here suggested that the silty material may be a loess like sediment (Pye 1995).

A pollen-based T_{Jul} reconstruction from northern Andøya indicates generally cold and humid conditions during the OD (Alm & Willassen 1993), whereas a slow but significant increase in T_{Jul} between 14 500–13 500 cal. a BP is indicated by pollen-based reconstructions from Bleiksvatnet and Brattheivatnet, northern Andøya (Aarnes *et al.* 2012; Birks *et al.* 2014).

(Units G1–3, F and E) – Minor short-lived glacier advances during the Allerød. – Allerød sediments are represented by the lithological units G(1–3), F and E, dated to 13 910±140–12 835±65 cal. a BP. The lithological units indicate a shifting environment within the catchment. During deposition of units G3 and G1, the glacier in Finnkongdalen was most likely melted away, whereas two very small glacier re-formations with a TPW-ELA of about 275 m a.s.l. are indicated by unit G2, between 13 820±135 and 13 530±95 cal. a BP. These glacier re-formations may be related to the IACP. On northern Andøya, pollen-based reconstructions indicate an increase in both T_{Jul} and humidity after a significant cooling during the IACP (Vorren *et al.* 1988; Alm 1993).

A more distinct glacier re-formation with a TPW-ELA of about 250 m a.s.l. during the LAC is indicated by the lithology in unit F, dated to 13 360±90–12 945±70 cal. a BP. The LAC glacier advance is similar to the OD glacier advance regarding the abrupt demise of the glacier.

The T_{Jul} reconstruction based on pollen from Lusvatnet shows a warming of 2.6 °C between 13 300–13 150 cal. a BP, and a subsequent cooling of 2 °C between 13 150 and 12 950 cal. a BP (Birks *et al.* 2014).

Hence, a significant increase in winter precipitation as snow is required to allow for a glacier re-formation during the LAC.

The lithology of unit G3 (13 910±140–13 820±135 cal. a BP), and especially of units G1 (13 530±95 to 13 360 cal. a BP) and E (12 945±70 to 12 835±65 cal. a BP), indicates that extra-glacial in-wash and *in situ* production/external input of organic material were the main depositional processes in Ner-Finnkongdalsvatnet. It is thus suggested that the glacier was most likely completely melted away during these periods.

Younger Dryas. – The YD deposits in Ner-Finnkongdalsvatnet are represented by units D(1–3), C and B, and are separated into five phases based on the relative input of interpreted glacier-derived sediments (Figs 6–8). The lithology in cores retrieved near the main inlet indicate a depositional regime more dominated by glacier activity between 12 835±65–11 645±200 cal. a BP, whereas the lithology of cores further away from the main inlet indicates a much more shifting depositional regime during this period. The ^{14}C-plateau in the period 12 350–11 700 cal. a BP with 1σ confidence intervals of up to 200 years must be taken into account when comparing the records from Ner-Finnkongdalsvatnet and Lusvatnet during the mid- to late YD (Reimer *et al.* 2020).

YD phase 1 (unit D3) – glacier re-formation. – During YD phase 1, between 12 835±65 and 12 500±65 cal. a BP, the interpreted lithology indicates glacier re-formation with steady growth and little influence from extra-glacial in-wash, except possibly between 12 690±35 and 12 790±40 cal. a BP. A local TPW-ELA of just above 180 m a.s.l. is reconstructed for the culmination of this glacier advance. The contemporaneous temperature reconstruction from Lusvatnet indicates a steady increase of 1.7 °C in T_{Jul} between 12 975 and 12 740 cal. a BP followed by a fairly stable T_{Jul} of ~8.2 °C until about 12 500 cal. a BP (Birks *et al.* 2014). The fact that an interpreted lowering of the local TPW-ELA early in YD phase 1 is contemporaneous to the temperature rise at Lusvatnet, implies a shift towards a more maritime climate with an increase in winter precipitation as snow on Andøya (Fig. 10D).

YD phase 2 (unit D2) – retreat with short-lived glacier advances. – The transition to YD phase 2 (12 500±115–12 250±210 cal. a BP) is marked by an abrupt change towards a shifting depositional environment with significant short-lived glacier fluctuations superimposed on a generally high level of extra-glacial in-wash. This shift is apparently synchronous with the onset of YD2 in Lusvatnet (Birks *et al.* 2014), which represents a period of highly fluctuating, yet generally decreasing T_{Jul}.

YD phase 3 (unit D1) – glacier advance. – YD phase 3 (12 250±210–12 150±235 cal. a BP) is characterized by a net lowering of the reconstructed local TPW-ELA to about 180 m a.s.l., and less extensive extra-glacial in-wash compared to glacial sources. The temperature record from Lusvatnet indicates a distinct increase of ~1.2 °C in T_{Jul}, but still rather low, within this phase (Birks *et al.* 2014).

YD phase 4 (unit C) – retreat with short-lived glacier advances. – The onset of YD phase 4 (12 150±235–11 810±220 cal. a BP) is similar to the transition between YD phases 1 and 2, as the depositional environment is significantly more unstable with an increase in extra-glacial sediments compared to glacial sources (Fig. 6).

The T_{Jul} from Lusvatnet indicates low temperatures during the early part of this phase until a gradual warming took place from about 12 000 cal. a BP (Birks *et al.* 2014). This may imply that the increased relative contribution of extra-glacial in-wash and *in situ* production/external input of organic material in Ner-Finnkongdalsvatnet is due to less glacier activity caused by increased continentality and related precipitation starvation.

YD phase 5 (unit B) – glacier advance to maximum extent. – There are no indications of extra-glacial in-wash in any of the cores from Ner-Finnkongdalsvatnet during YD phase 5 (11 810±220–11 645±200 cal. a BP). Hence, input of glacier-derived sediments caused by the most extensive glacier advance during the entire YD, with an ELA just below 180 m, is the most likely explanation. This glacier advance occurs contemporaneously with a gradual increase of ~1.4 °C in T_{Jul} at Lusvatnet (Birks *et al.* 2014). Similarly, the biostratigraphy of Jansvatnet, near Hammerfest in the northernmost region of Norway, suggests a significant warming from 11 850 cal. a BP until the end of the YD (Birks *et al.* 2012). Based on the Liestøl equation, such an increase in ablation season temperature implies a large increase in winter precipitation as snow at the ELA, thus indicating a shift towards a more maritime climate from around 11 800 cal. a BP and onwards. According to sediment parameters in all analysed cores from Ner-Finnkongdalsvatnet, the end of YD phase 5, dated to 11 645±200 cal. a BP, represents the final demise of the glacier in Finnkongdalen.

Stabilization of landscape at the YD–Holocene transition. – An abrupt demise of a glacier normally implies that a large area of previously ice-covered superficial sediments becomes available for remobilization and sedimentation in downstream lakes (Church & Ryder 1972; Ballantyne 2002; Orwin & Smart 2004). In addition to melting permafrost, the contribution of sediments related to such paraglacial activity cannot, however, be resolved directly by the currently used methods. The abrupt nature of the transition between a depositional environment dominated by glacially derived sediments before 11 645±110 cal. a BP and the

domination of sediments related to extra-glacial in-wash and *in situ* production/external input of organic material (from unit B to unit A in Figs 6 and 8), may indicate that the recently deglaciated landscape was rapidly stabilized. It is likely that the deglaciated upstream lake Øver-Finnkongdalsvatnet acted as an effective sediment trap, further reducing the effect of paraglacial activity on the depositional environment in lake Ner-Finnkongdalsvatnet.

A possible melt-out of permafrost in Finnkongdalen may be related to the period between about 11 000 to 10 500 cal. a BP with a weak lowering of the LOI related to a general increase in mean grain size, a large in-wash of medium and very fine silt and no increase in Ti (Figs 6, 7). Since this layer reflecting a possible melt-out of permafrost is only found in NFP 809 and not in NFP 409, it may be linked to the rock glacier in the SW-facing valley side of Finnkongdalen (Figs 2, 4).

Comparison with the SIS

The SIS reached the shelf edge west of Andøya twice during the LGM, before *c*. 26 cal. ka BP and between 23.5–22.2 cal. ka BP (Fig. 11; Vorren & Elvsborg 1979; Dahlgren & Vorren 2003; Rørvik *et al*. 2010; Rydningen *et al*. 2013; Vorren *et al*. 2013, 2015; Laberg *et al*. 2018; Alsos *et al*. 2020). Although there are no dated landforms in Finnkongdalen that can be related to these advances of the SIS, M1 could possibly represent a LGM glacier advance. The numerous efforts at environmental reconstructions based on biological indicators show a dry high-arctic climate throughout the LGM and the Lateglacial up until ~14.5 cal. ka BP (Alm 1993; Vorren *et al*. 2013). This is, however, punctuated by periods of warmer conditions, possibly allowing for growth of *Betula*, *Picea* and *Pinus* (Fig. 11C; Kullman 2006; Parducci *et al*. 2012; Vorren *et al*. 2013; Alsos *et al*. 2020). The suggested glacier advance in Finnkongdalen <21 970±615 cal. a BP, and the corresponding recession of the SIS are simultaneous with the Andøya thermomer 2 (22–20 cal. ka BP – Fig. 11; Alsos *et al*. 2020). It is thus suggested that a temperature increase induced a slight recession of the SIS, and a somewhat increased precipitation locally must have been a key driver of this particular glacial advance.

The YD glacier re-formation in Finnkongdalen fits quite well with the SIS advances during the early to mid-YD (Tromsø-Lyngen) (Fig. 11). As pointed out by Vorren & Plassen (2002), the distinct Tromsø-Lyngen glacier advance most likely started during the LAC in the late Allerød.

Implications for ocean–atmosphere changes in the North Atlantic region

Based on a comparison between the T_{Jul} record from Lusvatnet (Birks *et al*. 2014) and the local TPW-ELA reconstruction from Finnkongdalen, it is evident that drops in local TPW-ELAs during the LAC, YD phases 1, 3 and 5 are concurrent with reconstructed higher T_{Jul}. Likewise, high local TPW-ELAs in Finnkongdalen are apparently concurrent with reconstructed lower values of T_{Jul} around 13 500±50 cal. a BP, 12950±50 cal. a BP and during YD phase 4. Hence, periods during the Lateglacial with a more maritime climate with increased winter precipitation as snow during part of the year are suggested to be an important driver of glacier re-formations/advances. On the contrary, periods with a more continental climate with precipitation starvation are suggested to cause stagnation or complete demise of the glaciers.

Variations in YD sea-surface temperatures (SSTs) based on planktic foraminifera have been reconstructed from Andfjorden, approximately 50 km NE of Finnkongdalen (Figs 1, 10). The record indicates an extreme instability in SSTs between 12 800 and 11 500 cal. a BP, which is linked to shifting dominance between input of Atlantic water, periods with increased contribution of meltwater and prevailing cold (2–4 °C) Arctic water (Ebbesen & Hald 2004). Accordingly, sea-ice biomarkers in the same core indicate seasonal sea ice cover throughout the early to mid-YD, with decreasing sea-ice biomarker concentrations indicating a significant reduction in the spring sea-ice concentration during the late YD, between 11 900 and 11 500 cal. a BP (Cabedo-Sanz *et al*. 2013).

Similarly, a 'flickering' in the reconstructed input of glacial meltwater to the glacier-fed lake Kråkenes on the west coast of southern Norway (Fig. 1) has been related to decadal alternating sea ice cover and influx of warm North Atlantic waters through the Faroe-Shetland Channel after 12 100 cal. a BP (Fig. 10) (Bakke *et al*. 2009). This shift in depositional environment is apparently synchronous with the transition between the relatively stable YD phase 3 and YD phase 4, when the depositional environment alternated between glacial sedimentation and extra-glacial in-wash in Ner-Finnkongdalsvatnet (Fig. 10).

In contrast to the single marginal moraine suggested to have been formed by the late YD maximum glacier (phase 5) in Finnkongdalen, the reconstructed Kråkenes cirque glacier has left three sets of marginal moraines reflecting a successively smaller cirque glacier from the early, mid- and late YD, respectively (Larsen *et al*. 1984). The most likely explanation for these observations is enhanced precipitation starvation in Finnkongdalen during the early to mid-YD, while periodically increased precipitation is inferred on a decadal to centennial time scale at Kråkenes during the same time-span. It is suggested that the observed differences between Kråkenes and Finnkongdalen may reflect a north–south gradient in precipitation owing to the position of the arctic polar front and thus the meridional position of the polar jet stream and storm tracks in NW Europe during the YD. In that respect, the Arctic polar front resided

mainly to the south of Kråkenes before 12 100 cal. a BP, between Kråkenes and Andøya between 12 100 and 11 810±220 cal. a BP and possibly north of Andøya periodically after 11 810±220 cal. a BP. It is suggested that a relatively arid climate during the YD was caused by the SIS and the northern European plains in combination with extensive sea ice, as they produced blocking high-pressure systems, leading precipitation-bearing winds southwards (Rea *et al.* 2020).

Conclusions

Based on the above results and discussion, the following implications of local and regional importance are suggested.

- Marginal moraines have been used to reconstruct the maximum extent and local TPW-ELA for a local valley/cirque glacier in western Andøya, northern Norway. Two large glacier advances or halts during the Lateglacial after the LGM occurred during the OD and the YD. Adjusted for relative land uplift, the TPW-ELAs for the LGM, OD and YD are calculated to 134, 147 and 172 m a.s.l., respectively.
- A continuous local TPW-ELA curve for the Lateglacial is reconstructed, confirming significant glacier advance during the OD and the YD, and with minor advances during the IACP and the LAC.
- The catchment of Finnkongdalen was most likely deglaciated during the early Allerød between the OD and IACP, during the mid-Allerød between the IACP and the LAC, during the late Allerød between the LAC and the YD, and after the YD–Preboreal transition. Glacier activity was limited within the Bølling chronozone.
- Based on the continuous TPW-ELA record, the YD is subdivided into YD phases 1–5, where YD1, 3 and 5 are marked by relatively high glacier activity, whereas YD2 and 4 are marked by a relatively high influx of extra-glacial in-wash, which may result from mass-wasting events.
- Variations in mean annual precipitation as snow are reconstructed based on the Liestøl relationship. Significant increases in winter precipitation as snow are suggested to explain the glacier re-formation during the LAC, YD phase 1 and during the glacier advance to the maximum position in YD phase 5.
- A close link between meridional differences in precipitation, the position of storm tracks and inflow of North Atlantic waters during the mid- to late YD is suggested based on a comparison between the results from Finnkongdalen and S Norway. Hence, the storm tracks mostly passed south of S Norway during the early YD (before 12 100 cal. a BP), between S Norway and Andøya during the mid-YD (12 100–11 810±220 cal. a BP) and possibly north of Andøya during the late YD A(after 11 810±220 cal. a BP).

Acknowledgements. – We thank Sara Beate Aspen and Odd Inge Hesjedal Thorkildsen for help with GPR-profiling. The work with ^{10}Be benefited from internal funding from the Bjerknes Centre for Climate Research. HL thanks Maria Miguens-Rodriguez for assistance during laboratory processing of the samples. This research effort was supported by the Research Council of Norway funded ARCTREC (Arctic Records of Climate Change–dynamics, feedbacks and processes) project, coordinated by Eystein Jansen and Carin Andersson Dahl at the Bjerknes Centre for Climate Research, as well as by independent funding from the Research Council of Norway and the University of Bergen. HLJ thanks Inger G. Alsos, Jan Sverre Laberg and Liv Plassen for interesting discussions regarding past environmental changes and ice-sheet dynamics in coastal northern Norway. Thanks to Benjamin Aubrey Robson for language review. Thanks to reviewers Anders Schomacker and Eric Leonard for much appreciated comments, which helped to improve the manuscript. Thanks to the editor of *Boreas*, Jan A. Piotrowski for thoroughly reviewing the manuscript.

Author contributions. – HLJ, SOD and JB planned and designed the research. JB, SOD, BCK and HLJ carried out fieldwork; JB did the bathymetry and GPR measurements, HLJ, SOD, BCK and JB did the coring. HLJ did Quaternary geological mapping. BCK and HLJ did laboratory analyses on cores. HL carried out fieldwork, laboratory analysis and data analysis associated with ^{10}Be dates. HLJ carried out data analysis and wrote the manuscript, with major input from SOD and PRN. All co-authors commented on the manuscript.

Data availability statement. – Code used to run the age-depth model is described by Blaauw (2010) and can be downloaded from https://cran.r-project.org/web/packages/clam/index.html. Raw data from sediment analyses of grain size distribution, magnetic susceptibility, X-ray fluorescence and map data are available from the authors upon request. High resolution elevation (LIDAR) data (>2 pt m^{-2}) can be accessed at the Norwegian Mapping Authority's portal for elevation data (https://hoydedata.no/LaserInnsyn2/).

References

Aarnes, I., Bjune, A., Birks, H., Balascio, N., Bakke, J. & Blaauw, M. 2012: Vegetation responses to rapid climatic changes during the last deglaciation 13,500–8,000 years ago on southwest Andøya, arctic Norway. *Vegetation History and Archaeobotany 21*, 17–35.

Alm, T. 1993: Øvre Æråsvatn - palynostratigraphy of a 22,000 to 10,000 BP lacustrine record on Andøya, northern Norway. *Boreas 22*, 171–188.

Alm, T. & Birks, H. H. 1991: Late Weichselian flora and vegetation of Andøya, northern Norway-macrofossil (seed and fruit) evidence from Nedre Æråsvatn. *Nordic Journal of Botany 11*, 465–476.

Alm, T. & Willassen, E. 1993: Late weichselian chironomidae (diptera) stratigraphy of Lake Nedre Æråsvatn, Andøya, northern Norway. *Hydrobiologia 264*, 21–32.

Alsos, I. G., Sjögren, P., Brown, A. G., Gielly, L., Merkel, M. K. F., Paus, A., Lammers, Y., Edwards, M. E., Alm, T. & Leng, M. 2020: Last Glacial Maximum environmental conditions at Andøya, northern Norway; evidence for a northern ice-edge ecological "hotspot". *Quaternary Science Reviews 239*, 1–19.

Andersen, B. G. 1968: *Glacial Geology of Western Troms, North Norway.* 161 pp. Universitetsforlaget, Trondheim.

Andersen, B. G. 1975: Glacial geology of northern Nordland, north Norway. *Norges Geologiske Undersøkelse 320*, 1–74.

Andersen, J. L., Margreth, A., Fredin, O., Linge, H., Goodfellow, B. W., Faust, J. C., Knies, J., Solbakk, T., Brook, E. J., Scheiber, T., van der Lelij, R., Burki, V., Rubensdotter, L., Himmler, T., Yeşilyurt, S., Christl, M., Vockenhuber, C. & Akçar, N. 2022: Rapid post-glacial bedrock weathering in coastal Norway. *Geomorphology 397*, 1–19.

Anjar, J., Akçar, N., Lakeman, T., Larsen, E. A. & Seiler, M. 2021: ^{10}Be surface exposure dating of the deglaciation of northernmost Norway and Finland. *Boreas 50*, 369–380.

Bakke, J., Dahl, S. O., Paasche, Ø., Løvlie, R. & Nesje, A. 2005: Glacier fluctuations, equilibrium-line altitudes and palaeoclimate in Lyngen,

northern Norway, during the Lateglacial and Holocene. *The Holocene 15*, 518–540.
Bakke, J., Dahl, S. O., Paasche, Ø., Simonsen, J. R., Kvisvik, B., Bakke, K. & Nesje, A. 2010: A complete record of Holocene glacier variability at Austre Okstindbreen, northern Norway: an integrated approach. *Quaternary Science Reviews 29*, 1246–1262.
Bakke, J., Lie, Ø., Heegaard, E., Dokken, T., Haug, G. H., Birks, H. H., Dulski, P. & Nilsen, T. 2009: Rapid oceanic and atmospheric changes during the Younger Dryas cold period. *Nature Geoscience 2*, 202–205.
Bakke, J., Trachsel, M., Kvisvik, B. C., Nesje, A. & Lyså, A. 2013: Numerical analyses of a multi-proxy data set from a distal glacier-fed lake, Sørsendalsvatn, western Norway. *Quaternary Science Reviews 73*, 182–195.
Balco, G., Stone, J. O., Lifton, N. A. & Dunai, T. J. 2008: A complete and easily accessible means of calculating surface exposure ages or erosion rates from ^{10}Be and ^{26}Al measurements. *Quaternary Geochronology 3*, 174–195.
Ballantyne, C. K. 2002: A general model of paraglacial landscape response. *The Holocene 12*, 371–376.
Benn, D. I. & Hulton, N. R. J. 2010: An Excel™ spreadsheet program for reconstructing the surface profile of former mountain glaciers and ice caps. *Computers & Geosciences 36*, 605–610.
Benn, D. I. & Lehmkuhl, F. 2000: Mass balance and equilibrium-line altitudes of glaciers in high-mountain environments. *Quaternary International 65–66*, 15–29.
Birks, H. J. B. 1987: Multivariate analysis of stratigraphic data in geology: a review. *Chemometrics and Intelligent Laboratory Systems 2*, 109–126.
Birks, H., Battarbee, R. W. & Birks, H. J. B. 2000: The development of the aquatic ecosystem at Kråkenes Lake, western Norway, during the late glacial and early Holocene - a synthesis. *Journal of Paleolimnology 23*, 91–114.
Birks, H. H., Aarnes, I., Bjune, A. E., Brooks, S. J., Bakke, J., Kühl, N. & Birks, H. J. B. 2014: Lateglacial and early-Holocene climate variability reconstructed from multi-proxy records on Andøya, northern Norway. *Quaternary Science Reviews 89*, 108–122.
Birks, H. H., Jones, V. J., Brooks, S. J., Birks, H. J. B., Telford, R. J., Juggins, S. & Peglar, S. M. 2012: From cold to cool in northernmost Norway: Lateglacial and early Holocene multi-proxy environmental and climate reconstructions from Jansvatnet, Hammerfest. *Quaternary Science Reviews 33*, 100–120.
Blaauw, M. 2010: Methods and code for 'classical' age-modelling of radiocarbon sequences. *Quaternary Geochronology 5*, 512–518.
Blikra, L. H. & Nemec, W. 1998: Postglacial colluvium in western Norway: depositional processes, facies and palaeoclimatic record. *Sedimentology 45*, 909–959.
Blott, S. J. & Pye, K. 2001: GRADISTAT: a grain size distribution and statistics package for the analysis of unconsolidated sediments. *Earth Surface Processes and Landforms 26*, 1237–1248.
Borchers, B., Marrero, S., Balco, G., Caffee, M., Goehring, B., Lifton, N., Nishiizumi, K., Phillips, F., Schaefer, J. & Stone, J. 2016: Geological calibration of spallation production rates in the CRONUS-Earth project. *Quaternary Geochronology 31*, 188–198.
Cabedo-Sanz, P., Belt, S. T., Knies, J. & Husum, K. 2013: Identification of contrasting seasonal sea ice conditions during the Younger Dryas. *Quaternary Science Reviews 79*, 74–86.
Child, D., Elliott, G., Mifsud, C., Smith, A. M. & Fink, D. 2000: Sample processing for earth science studies at ANTARES. *Nuclear Instruments and Methods in Physics Research Section B: Beam Interactions with Materials and Atoms 172*, 856–860.
Church, M. & Ryder, J. M. 1972: Paraglacial sedimentation: a consideration of fluvial processes conditioned by glaciation. *Geological Society of America Bulletin 83*, 3059–3072.
Croudace, I. W., Rindby, A. & Rothwell, R. G. 2006: ITRAX: description and evaluation of a new multi-function X-ray core scanner. *In* Rothwell, R. G. (ed.): *New Techniques in Sediment Core Analysis*, 51–63. Geological Society, London.
Dahl, S. O. & Nesje, A. 1992: Paleoclimatic implications based on equilibrium-line altitude depressions of reconstructed Younger Dryas and Holocene cirque glaciers in inner Nordfjord, western Norway. *Palaeogeography, Palaeoclimatology, Palaeoecology 94*, 87–97.
Dahl, S. O. & Nesje, A. 1996: A new approach to calculating Holocene winter precipitation by combining glacier equilibrium-line altitudes and pine-tree limits: a case study from Hardangerjøkulen, central southern Norway. *The Holocene 6*, 381–398.
Dahl, S. O., Bakke, J., Lie, Ø. & Nesje, A. 2003: Reconstruction of former glacier equilibrium-line altitudes based on proglacial sites: an evaluation of approaches and selection of sites. *Quaternary Science Reviews 22*, 275–287.
Dahl, S. O., Nesje, A. & Øvstedal, J. 1997: Cirque glaciers as morphological evidence for a thin Younger Dryas ice sheet in east-central southern Norway. *Boreas 26*, 161–180.
Dahlgren, K. T. & Vorren, T. O. 2003: Sedimentary environment and glacial history during the last 40 ka of the Vøring continental margin, mid-Norway. *Marine Geology 193*, 93–127.
Dunne, J., Elmore, D. & Muzikar, P. 1999: Scaling factors for the rates of production of cosmogenic nuclides for geometric shielding and attenuation at depth on sloped surfaces. *Geomorphology 27*, 3–11.
Ebbesen, H. & Hald, M. 2004: Unstable Younger Dryas climate in the northeast North Atlantic. *Geology 32*, 673–676.
Elverland, E. & Alm, T. 2012: *Late Weichselian to early Holocene vegetation and bird activity on Andøya, Nordland County: as evidenced primarily by macrofossils.* Fakultet for biovitenskap, fiskeri og økonomi, University of Tromsø, Tromsø.
Engen-Skaugen, T. & Tveito, O. E. 2007: Spatially distributed temperature lapse rate in Fennoscandia. *In* Szalai, S., Bihari, Z., Szentimrey, T. & Lakatos, M. (eds.): *Spatial Interpolation in Climatology and Meteorology*, 93–100. COST Office, Luxembourg.
Fjellberg, A. 1978: Fragments of a middle Weichselian fauna on Andøya, north Norway. *Boreas 7*, p. 39.
Gosse, J. C. & Phillips, F. M. 2001: Terrestrial in situ cosmogenic nuclides: theory and application. *Quaternary Science Reviews 20*, 1475–1560.
Haug, G. H., Hughen, K. A., Sigman, D. M., Peterson, L. C. & Rohl, U. 2001: Southward migration of the intertropical convergence zone through the Holocene. *Science 293*, 1304–1308.
Heiri, O., Lotter, A. F. & Lemcke, G. 2001: Loss on ignition as a method for estimating organic and carbonate content in sediments: reproducibility and comparability of results. *Journal of Paleolimnology 25*, 101–110.
Henningsen, T. & Tveten, E. 1998: *Berggrunnskart Andøya, M 1:250000*. Geologisk kart over Norge, Norges geologiske undersøkelse.
Humlum, O. 1998: The climatic significance of rock glaciers. *Permafrost and Periglacial Processes 9*, 375–395.
Johnsen, M. S. 2020: Erosjonsrater og landskapsuvikling på Andøya, Vesterålen. Unpublished thesis, Department of Geoscience, University of Bergen.
Karlén, W. 1976: Lacustrine sediments and tree-limit variations as indicators of Holocene climatic fluctuations in Lappland, northern Sweden. *Geografiska Annaler Series A-Physical Geography 58*, 1–34.
Karlén, W. 1981: Lacustrine sediment studies - a technique to obtain a Continous record of Holocene glacier variations. *Geografiska Annaler Series A-Physical Geography 63*, 273–281.
Kartverket 2022: *hoydedata.no*. https://hoydedata.no/ (accessed 12.01.2022).
Kohl, C. P. & Nishiizumi, K. 1992: Chemical isolation of quartz for measurement of in-situ-produced cosmogenic nuclides. *Geochimica et Cosmochimica Acta 56*, 3583–3587.
Kullman, L. 2006: Late-glacial trees from arctic coast to alpine tundra: response to Birks et al. 2005 and 2006. *Journal of Biogeography 33*, 377–378.
Kutzbach, J., Liu, X., Liu, Z. & Chen, G. 2008: Simulation of the evolutionary response of global summer monsoons to orbital forcing over the past 280,000 years. *Climate Dynamics 30*, 567–579.
Laberg, J. S., Eilertsen, R. S. & Salomonsen, G. R. 2018: Deglacial dynamics of the Vestfjorden–Trænadjupet palaeo-ice stream, northern Norway. *Boreas 47*, 225–237.
Larsen, S. B. 2010: Bruk av GPR for å auke forståinga av sedimentasjonsprosessar i Nedre Finnkongdalsvatn, Andøy, Nord-Norge. Unpublished thesis, Department of Geography, University of Bergen, Bergen.

Larsen, E., Eide, F., Longva, O. & Mangerud, J. 1984: Allerød-Younger Dryas climatic inferences from cirque glaciers and vegetational development in the Nordfjord area, Western Norway. *Arctic and Alpine Research 16*, 137–160.
Leclercq, P. & Oerlemans, J. 2012: Global and hemispheric temperature reconstruction from glacier length fluctuations. *Climate Dynamics 38*, 1065–1079.
Lie, Ø. & Paasche, Ø. 2006: How extreme was northern hemisphere seasonality during the Younger Dryas? *Quaternary Science Reviews 25*, 404–407.
Liestøl, O. 1967: Storbreen glacier in Jotunheimen, Norway. *Norsk Polarinstitutt Skrifter 141*, 1–63.
Lifton, N., Sato, T. & Dunai, T. J. 2014: Scaling in situ cosmogenic nuclide production rates using analytical approximations to atmospheric cosmic-ray fluxes. *Earth and Planetary Science Letters 386*, 149–160.
Mangerud, J. & Berglund, B. E. 1978: The subdivision of the Quaternary of Norden: a discussion. *Boreas 7*, 179–181.
Marrero, S. M., Phillips, F. M., Caffee, M. W. & Gosse, J. C. 2016: CRONUS-Earth cosmogenic 36Cl calibration. *Quaternary Geochronology 31*, 199–219.
MET 2021: *Monthly mean temperature and precipitation. AD1900-2021, Station no. 87100*. Klimaservicesenter, https://seklima.met.no/.
Moe, K. 2009: Reconstruction of local glaciers and climate in Nøssdalsvatn catchment on central Andøy, northern Norway. Unpublished thesis, Department of Geography, University of Bergen, Bergen.
Møller, J. J. 1989: Geometric simulation and mapping of Holocene relative sea-level changes in northern Norway. *Journal of Coastal Research 5*, 403–417.
Møller, J. J., Danielsen, T. K. & Fjalstad, A. 1992: Late Weichselian glacial maximum on Andøya, North Norway. *Boreas 21*, 1–13.
Nesje, A. 1992a: A piston corer for lacustrine and marine-sediments. *Arctic and Alpine Research 24*, 257–259.
Nesje, A. 1992b: Topographical effects on the equilibrium-line altitude on glaciers. *GeoJournal 27*, 383–391.
Nesje, A. & Dahl, S. O. 2003: Glaciers as indicators of Holocene climate change. *In* Mackay, A., Battarbee, R., Birks, H. J. B. & Oldfield, F. (eds.): *Global Change in the Holocene*, 264–280. Hodder Arnold, London.
Nesje, A., Bakke, J., Dahl, S. O., Lie, Ø. & Matthews, J. A. 2008: Norwegian mountain glaciers in the past, present and future. *Global and Planetary Change 60*, 10–27.
Nesje, A., Matthews, J. A., Dahl, S. O., Berrisford, M. S. & Andersson, C. 2001: Holocene glacier fluctuations of Flatebreen and winter-precipitation changes in the Jostedalsbreen region, western Norway, based on glaciolacustrine sediment records. *The Holocene 11*, 267–280.
Nielsen, P. R., Balascio, N. L., Dahl, S. O., Jansen, H. L., Støren, E. W. & Bradley, R. S. 2016a: A high-resolution 1200-year lacustrine record of glacier and climate fluctuations in Lofoten, northern Norway. *The Holocene 26*, 917–934.
Nielsen, P. R., Dahl, S. O., Jansen, H. L. & Støren, E. N. 2016b: Holocene aeolian sedimentation and episodic mass-wasting events recorded in lacustrine sediments on Langøya in Vesterålen, northern Norway. *Quaternary Science Reviews 148*, 146–162.
NIST, C. 1990: *Radioactivity Standard*. SRM 4325.
Nye, J. 1952: The mechanics of glacier flow. *Journal of Glaciology 2*, 82–93.
Oien, R. P., Rea, B. R., Spagnolo, M., Barr, I. D. & Bingham, R. G. 2021: Testing the area–altitude balance ratio (AABR) and accumulation–area ratio (AAR) methods of calculating glacier equilibrium-line altitudes. *Journal of Glaciology 68*, 357–368.
Orwin, J. F. & Smart, C. C. 2004: The evidence for paraglacial sedimentation and its temporal scale in the deglacierizing basin of Small River Glacier, Canada. *Geomorphology 58*, 175–202.
Osmaston, H. 2005: Estimates of glacier equilibrium line altitudes by the Area×Altitude, the Area×Altitude Balance Ratio and the Area×Altitude Balance Index methods and their validation. *Quaternary International 138*, 22–31.
Paasche, Ø., Dahl, S. O., Bakke, J., Løvlie, R. & Nesje, A. 2007: Cirque glacier activity in arctic Norway during the last deglaciation. *Quaternary Research 68*, 387–399.
Pailard, D., Labeyrie, L. & Yiou, P. 1996: Macintosh Program performs time-series analysis. *Eos, Transactions, American Geophysical Union 77*, p. 379.
Parducci, L., Edwards, M. E., Bennett, K. D., Alm, T., Elverland, E., Tollefsrud, M. M., Jørgensen, T., Houmark-Nielsen, M., Larsen, N. K. & Kjær, K. H. 2012: Response to comment on "Glacial survival of boreal trees in northern Scandinavia". *Science 338*, p. 742.
Pellitero, R., Rea, B. R., Spagnolo, M., Bakke, J., Ivy-Ochs, S., Hughes, P., Lukas, S. & Ribolini, A. 2015: A GIS tool for automatic calculation of glacier equilibrium-line altitudes. *Computers & Geosciences 82*, 55–62.
Porter, S. C. 1975: Equilibrium-line altitudes of the late Quaternary glaciers in the Southern Alps, New Zealand. *Quaternary Research 5*, 27–47.
Pye, K. 1995: The nature, origin and accumulation of loess. *Quaternary Science Reviews 14*, 653–667.
R Core Team. 2021: *R: A language and Environment for Statistical Computing*. R Foundation for Statistical Computing, Vienna, Austria. Available at: https://www.R-project.org/.
Rasmussen, A. 1984: Late Weichselian moraine chronology of the Vesterålen islands, North Norway. *Norsk Geologisk Tidsskrift 64*, 193–219.
Rea, B. R. 2009: Defining modern day Area-Altitude Balance Ratios (AABRs) and their use in glacier-climate reconstructions. *Quaternary Science Reviews 28*, 237–248.
Rea, B. R., Pellitero, R., Spagnolo, M., Hughes, P., Ivy-Ochs, S., Renssen, H., Ribolini, A., Bakke, J., Lukas, S. & Braithwaite, R. J. 2020: Atmospheric circulation over Europe during the Younger Dryas. *Science Advances 6*, eaba4844, https://doi.org/10.1126/sciadv.aba4844.
Reimer, P. J. and 41 others 2020: The IntCal20 northern hemisphere radiocarbon age calibration curve (0–55 cal kBP). *Radiocarbon 62*, 725–757.
Rørvik, K.-L., Laberg, J., Hald, M., Ravna, E. & Vorren, T. 2010: Behavior of the northwestern part of the Fennoscandian Ice Sheet during the Last Glacial Maximum–a response to external forcing. *Quaternary Science Reviews 29*, 2224–2237.
Rydningen, T. A., Vorren, T. O., Laberg, J. S. & Kolstad, V. 2013: The marine-based NW Fennoscandian ice sheet: glacial and deglacial dynamics as reconstructed from submarine landforms. *Quaternary Science Reviews 68*, 126–141.
Schilling, D. H. & Hollin, J. T. 1981: Numerical reconstructions of valley glaciers and small ice caps. *In* Denton, G. H. & Hughes, T. J. (eds.): *The Last Great Ice Sheets*, 207–220. Wiley, New York.
Serreze, M. C. & Barry, R. G. 2011: Processes and impacts of Arctic amplification: a research synthesis. *Global and Planetary Change 77*, 85–96.
Thompson, R., Battarbee, R. W., O'Sullivan, P. E. & Oldfield, F. 1975: Magnetic susceptibility of Lake sediments. *Limnology and Oceanography 20*, 687–698.
Vasskog, K., Nesje, A., Støren, E. N., Waldmann, N., Chapron, E. & Ariztegui, D. 2011: A Holocene record of snow-avalanche and flood activity reconstructed from a lacustrine sedimentary sequence in Oldevatnet, western Norway. *The Holocene 21*, 597–614.
Vasskog, K., Paasche, Ø., Nesje, A., Boyle, J. F. & Birks, H. J. B. 2012: A new approach for reconstructing glacier variability based on lake sediments recording input from more than one glacier. *Quaternary Research 77*, 192–204.
Vorren, K.-D. 1978: Late and middle Weichselian stratigraphy of Andøya, north Norway. *Boreas 7*, 19–38.
Vorren, T. O. & Elvsborg, A. 1979: Late Weichselian deglaciation and paleoenvironment of the shelf and coastal areas of Troms, north Norway-a review. *Boreas 8*, 247–253.
Vorren, T. O. & Plassen, L. I. V. 2002: Deglaciation and palaeoclimate of the Andfjord-Vågsfjord area, North Norway. *Boreas 31*, 97–125.
Vorren, K.-D., Elverland, E., Blaauw, M., Ravna, E. K. & Jensen, C. A. H. 2009: Vegetation and climate c. 12 300–9000 cal. yr BP at Andøya, NW Norway. *Boreas 38*, 401–420.
Vorren, T. O., Rydningen, T. A., Baeten, N. J. & Laberg, J. S. 2015: Chronology and extent of the Lofoten–Vesterålen sector of the

Scandinavian Ice Sheet from 26 to 16 cal. ka BP. *Boreas 44*, 445–458.
Vorren, T. O., Vorren, K. D., Alm, T., Gulliksen, S. & Lovlie, R. 1988: The Last Deglaciation (20,000 to 11,000 bp) on Andøya, northern Norway. *Boreas 17*, 41–77.
Vorren, T. O., Vorren, K.-D., Aasheim, O., Dahlgren, K. I. T., Forwick, M. & Hassel, K. 2013: Palaeoenvironment in northern Norway between 22.2 and 14.5 cal. ka BP. *Boreas 42*, 876–895.
Webb, P. A. & Orr, C. 1997: *Analytical Methods in Fine Particle Technology*. 374 pp. Micromeritics Instrument Corp, Norcross.
Weibull, J., Enander, H., Sandvik, G., Joys, C. & Christensen, J. 2022: *Norway*. https://www.britannica.com/place/Norway/Climate (accessed 12.10.2022).
Wittmeier, H. E., Schaefer, J. M., Bakke, J., Rupper, S., Paasche, Ø., Schwartz, R. & Finkel, R. C. 2020: Late glacial mountain glacier culmination in Arctic Norway prior to the Younger Dryas. *Quaternary Science Reviews 8*, 13, https://doi.org/10.1016/j.quascirev.2020.106461.
Xu, S., Dougans, A. B., Freeman, S. P. H. T., Schnabel, C. & Wilcken, K. M. 2010: Improved Be-10 and Al-26 AMS with a 5 MV spectrometer. *Nuclear Instruments and Methods B 268*, 736–738.

Supporting Information

Additional Supporting Information to this article is available at http://www.boreas.dk.

Table S1. Correlation matrix with key sediment parameters analysed in NFP 409 and NFP 809.

Data S1. Laboratory analysis and calculation of ^{10}Be ages.